

**UNIVERSITY OF GAZIANTEP
GRADUATE SCHOOL OF
NATURAL & APPLIED SCIENCES**

**ULTRA-THIN ENGINEERED
CEMENTITIOUS COMPOSITES OVERLAY
SYSTEMS FOR REHABILITATION OF
RIGID CONCRETE PAVEMENTS**

**M. Sc. THESIS
IN
CIVIL ENGINEERING**

**BY
HISHAM JASHAMI
JUNE 2012**

**Ultra-Thin Engineered Cementitious Composites
Overlay Systems for Rehabilitation of Rigid Concrete
Pavements**

**M.Sc. Thesis
In
Civil Engineering
University of Gaziantep**

**Supervisor
Assoc. Prof. Dr. Mustafa ŞAHMARAN**

**by
Hisham JASHAMI
June 2012**

© 2012 [Hisham JASHAMĪ].

T.C.
UNIVERSITY OF GAZİANTEP
GRADUATE SCHOOL OF
NATURAL & APPLIED SCIENCES
CIVIL ENGINEERING DEPARTMENT

Name of the thesis: Ultra-Thin Engineered Cementitious Composites Overlay
Systems for Rehabilitation of Rigid Concrete Pavements

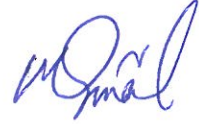
Name of the student: Hisham JASHAMI
Exam date: June 4, 2012

Approval of the Graduate School of Natural and Applied Sciences



Prof. Dr. Ramazan KOÇ
Director

I certify that this thesis satisfies all the requirements as a thesis for the degree of
Master of Science.



Prof. Dr. Mustafa GÜNAL
Head of Department

This is to certify that we have read this thesis and that in our opinion it is fully
adequate, in scope and quality, as a thesis for the degree of Master of Science.



Assoc. Prof. Dr. Mustafa ŞAHMARAN
Supervisor

Examining Committee Members

Signature

Assoc. Prof. Dr. Aytaç GÜVEN



Assist. Prof. Dr. Ömer PAYDAK



Assoc. Prof. Dr. Mustafa ŞAHMARAN



T.C.
UNIVERSITY OF GAZİANTEP
GRADUATE SCHOOL OF
NATURAL & APPLIED SCIENCES
CIVIL ENGINEERING DEPARTMENT

Name of the thesis: Ultra-Thin Engineered Cementitious Composites Overlay
Systems for Rehabilitation of Rigid Concrete Pavements

Name of the student: Hisham JASHAMI
Exam date: June 4, 2012

Approval of the Graduate School of Natural and Applied Sciences

Prof. Dr. Ramazan KOÇ
Director

I certify that this thesis satisfies all the requirements as a thesis for the degree of
Master of Science.

Prof. Dr. Mustafa GÜNAL
Head of Department

This is to certify that we have read this thesis and that in our opinion it is fully
adequate, in scope and quality, as a thesis for the degree of Master of Science.

Assoc. Prof. Dr. Mustafa ŞAHMARAN
Supervisor

Examining Committee Members

Signature

Assoc. Prof. Dr. Aytaç GÜVEN

Assist. Prof. Dr. Ömer PAYDAK

Assoc. Prof. Dr. Mustafa ŞAHMARAN

I hereby declare that all information in this document has been obtained and presented in accordance with academic rules and ethical conduct. I also declare that, as required by these rules and conduct, I have fully cited and referenced all material and results that are not original to this work.



Hisham JASHAMI

I hereby declare that all information in this document has been obtained and presented in accordance with academic rules and ethical conduct. I also declare that, as required by these rules and conduct, I have fully cited and referenced all material and results that are not original to this work.

Hisham JASHAMI

ABSTRACT

Ultra-Thin Engineered Cementitious Composites Overlay Systems for Rehabilitation of Rigid Concrete Pavements

JASHAMI, Hisham

M.Sc. in Civil Engineering

Supervisor: Assoc. Prof. Dr. Mustafa ŞAHMARAN

June 2012, 71 pages

In recent years, the use of rigid concrete overlay has become increasingly popular in bridge deck, highway and airport pavements and industrial floor rehabilitation. The main purpose of an overlay is to extend the service life of the structure by providing protection from the penetration of aggressive agents and water and a durable wearing surface. Moreover the overlay provides adequate load bearing capacity, which is compatible with the loading of the pavement and bridge deck. The superior ductility and improved durability characteristics of Engineered Cementitious Composites (ECC) suggest that they could be used as an attractive alternative to conventional overlay materials. In this study, the performance of ECC as pavement overlay material with different thicknesses is investigated. Two different ECC-overlay mixture designs are investigated: one with high strength and moderate ductility, and the other with moderate strength and high ductility. Micro-silica concrete (MSC), generally used as overlay material, is also prepared as a control mixture. For monolithic specimens, compressive strength, flexural strength, drying shrinkage and restrained shrinkage, and for layered specimens flexural strength and reflective cracking characteristics are investigated as performance criterias, respectively. The test results show that, for the same geometry and loading conditions, layered ECC beams have a significantly increase of both load carrying capacity and deformability by deflection at ultimate load, and shows better crack width control in comparison with MSC composite beam.

Keywords: Pavement overlay, Engineered Cementitious Composites (ECC), Reflective cracking, Flexural performance.

ÖZET

Rijit Beton Kaplamaların Onarımı için Tasarlanmış Çok İnce Çimento Bağlayıcılı Kompozit Kaplama Sistemleri

JASHAMI, Hisham

Yüksek Lisans Tezi, İnşaat Mühendisliği Bölümü

Tez Yöneticisi: Doç. Dr. Mustafa ŞAHMARAN

Haziran 2012, 71 sayfa

Son yıllarda, köprü tabliyeleri, otoyollar, havaalanı kaplamaları ve endüstriyel zeminlerin onarımında rijit beton kaplamaların kullanımı hızla artmaktadır. Bir kaplamanın temel amacı, zararlı maddelerin ve suyun girişini engelleyerek yapının servis ömrünü uzatmak ve dayanıklı aşınma yüzeyi sağlamaktır. Ayrıca, kaplama, döşeme ve köprü tabliyelerinin yüklenme durumlarına uyumlu olarak yeterli yük taşıma kapasitesi sağlar. Tasarlanmış Çimento Bağlayıcılı Kompozitlerin (ECC) üstün süneklik ve dayanıklılık özelliklerinden dolayı, bu malzemeleri geleneksel kaplama malzemelerinin yerine kullanılabilir önemli bir alternatif kaplama malzemesi olmasını sağlamaktadır. Bu çalışmada, kaplama malzemesi olarak kullanılan farklı kalınlıklara sahip ECC'nin performansı incelenmiştir. İki farklı ECC-kaplama karışımı incelenmiştir: birinci karışım, yüksek dayanım ve orta derecede süneklik, ikinci karışım ise orta dayanım ve yüksek süneklik özelliklerine sahiptir. Ayrıca, kontrol karışımı olarak genel kaplama malzemesi olarak kullanılan mikro-silis betonu (MSB) üretilmiştir. Performans kriterleri olarak, monolitik numunelerde basınç ve eğilmede çekme dayanımı, kuruma ve kısıtlanmış rötre ve tabakalı numunelerde ise eğilmede çekme dayanımı ve yansıma çatlakları özellikleri araştırılmıştır. Test sonuçları, aynı geometrik ölçüler ve yükleme koşulları altında, tabakalı ECC kirişlerinin kompozit MSB numunelerine kıyasla yük taşıma kapasitesini ve maksimum yükleme altındaki şekil değiştirme özelliğini önemli ölçüde iyileştirdiğini göstermektedir.

Anahtar Kelimeler: Döşeme kaplaması, Tasarlanmış Çimento Bağlayıcılı Kompozitler (ECC), Yansıma çatlakları, Eğilmede çekme dayanımı performansı.

ACKNOWLEDGEMENT

This dissertation has been completed under the guidance of my great teacher and advisor, Assoc. Prof. Dr. Mustafa ŞAHMARAN. Without his support, inspiration, dedication of time and energy throughout the past year, I could have never completed this work. I owe forever my sincerest gratitude to him, for opening my eyes to the innovative material technology world, and for challenging me with novel research ideas capable of solving real-world problems. His technical insight was priceless.

I thank Republic of Iraq Ministry of Higher Education and Iraq Culture Attache in Ankara for their help during my study in Turkey.

I must acknowledge the financial assistance of the Scientific and Technical Council of Turkey (TÜBİTAK) provided under Project: MAG-108M495 and Gaziantep University Scientific Research Centre provided under Project: MF.10.09.

My deep appreciations and thanks to Research Assistant Hasan Erhan YÜCEL and Gürkan YILDIRIM for their help and valuable guidance during the entire work.

Special thanks to my committee: Assoc. Prof. Dr. Aytaç GÜVEN and Assist. Prof. Dr. Ömer PAYDAK for their encouragement and insightful comments.

My sincere appreciation also extends to all my friends, especially Ali, Abdulrahman and Haider.

I would also like to thank my family: my sister, her husband and my uncle for their love, support and encouragement during my study.

Finally, I would like to dedicate this thesis to my amazing mother, the woman who illuminated my path, supported, encouraged and inspired me throughout my life.

TABLE OF CONTENTS

	Page
ABSTRACT	v
ÖZET	vi
ACKNOWLEDGEMENT.....	vii
TABLE OF CONTENTS.....	viii
LIST OF FIGURES	xi
LIST OF TABLES.....	xiv
LIST OF SYMBOLS/ABBREVIATIONS.....	xv
CHAPTER I.....	1
INTRODUCTION	1
1.1 General	1
1.2 Research Objectives and Scope	3
CHAPTER II	5
LITERATURE REVIEW AND BACKGROUND	5
2.1 Introduction.....	5
2.2 Proposed Material Solution for Sustainable Pavement Overlay.....	6
2.3. Engineered Cementitious Composites (ECC)	10
2.3.1 Background of Engineered Cementitious Composites	10
2.3.2 Design of Engineered Cementitious Composites.....	12

2.4 Use of ECC as an Overlay Material.....	14
2.4.1 Mechanical and Environmental Performance of ECC in Pavement Applications.....	15
2.4.1.1 Shrinkage.....	16
2.4.1.2 Fatigue Testing and Overlay Bond Characteristics.....	16
2.4.1.3 Freeze-Thaw and Salt Scaling Resistance.....	17
2.4.1.4 Abrasion and Wear Testing.....	20
2.4.1.5 Early Age Strength.....	20
2.4.1.6 Long Term Strain Capacity.....	21
2.4.1.7 Accelerated Weathering Tests.....	22
2.4.2 Cost of ECC Materials.....	22
CHAPTER III.....	24
EXPERIMENTAL PROGRAM.....	24
3.1 Materials.....	24
3.1.1 Portland Cement.....	24
3.1.2 Mineral Admixtures.....	25
3.1.2.1 Fly Ash.....	25
3.1.2.2 Slag.....	25
3.1.2.3 Micro-silica.....	26
3.1.3 Aggregate.....	27
3.1.4 Chemical Admixtures.....	28
3.1.5 Polyvinyl Alcohol (PVA) Fiber.....	28
3.2 Mixtures Proportions.....	29
3.3 Specimens Preparation.....	32
3.4 Test Procedure for Overlay Materials.....	33
3.4.1 Compressive Strength.....	33
3.4.2 Flexural Performance.....	34
3.4.3 Drying Shrinkage.....	35
3.4.4 Restrained Ring Shrinkage.....	36

3.5 Specimen Preparation and Testing for Flexural Performances and Reflective Cracking of Layered Specimens (Overlay+Substrate Concrete).....	37
3.5.1 Flexural Performance of Layered Specimens	37
3.5.2 Reflective Cracking of Layered Specimens.....	39
CHAPTER IV	42
RESULTS AND DISCUSSIONS.....	42
4.1 Properties of Overlay Materials	42
4.1.1 Compressive Strength.....	42
4.1.2 Flexural Strength	43
4.1.3 Drying Shrinkage	45
4.1.4 Restrained Shrinkage Cracking	47
4.2 Properties of Overlaid Specimens.....	50
4.2.1 Flexural Performance	50
4.2.2 Reflective Cracking Test	54
CHAPTER V	61
CONCLUSIONS.....	61
REFERENCES	63

LIST OF FIGURES

	Page
Figure 2.1 Tensile behavior of plain and fiber reinforced cementitious materials.....	7
Figure 2.2 Typical tensile stress-strain curve and crack width development of ECC (Weimann and Li, 2003b)	11
Figure 2.3 Response of ECC under flexural loading	12
Figure 2.4 Crack bridging stress versus crack opening relation.....	13
Figure 2.5 Crack Width Development as a Function of Drying Time (RH=50%) (Weimann and Li, 2003a).	16
Figure 2.6 ECC specimen surface appearance after (a) normal curing and (b) freeze- thaw cycles	18
Figure 2.7 Mass of scaled-off particles versus number of freeze thaw cycles for virgin mortar and virgin ECC prisms in presence of de-icing salts (Şahmaran and Li, 2007).....	19
Figure 2.8 Tensile strain capacity development of ECC material (Li and Lepech, 2004).	21
Figure 3.1 Particle size distributions of Portland cement, fly ash, slag and silica fume.	25
Figure 3.2 Particle morphology of Portland cement, micro-silica, fly ash and slag determined by SEM	26
Figure 3.3 The grain size distribution curves for the aggregates used in this study...	27
Figure 3.4 PVA Fiber used in the production of ECC	28

Figure 3.5 Production of ECC by using Hobart Type mixer	32
Figure 3.6 Curing of ECC specimens after production of them.....	33
Figure 3.7 Compression testing machine with a cylinder sample	33
Figure 3.8 Four-point bending test	34
Figure 3.9. Four-point flexural strength test	35
Figure 3.10 Drying shrinkage device and samples.....	36
Figure 3.11 Restrained shrinkage test setup.....	37
Figure 3.12 Substrate specimen with 30 mm thickness after diamond saw cutting ...	38
Figure 3.13 Layered specimens with different thicknesses for flexural performance	39
Figure 3.14 Substrate specimen after cutting (30 mm thickness) with a vertical crack	40
Figure 3.15 Model of four-point bending for reflective cracking test	41
Figure 4.1 Flexural strength-mid-span beam deflection curves of overlay materials at 28 days of age.....	44
Figure 4.2 Drying shrinkages of overlay mixtures	46
Figure 4.3 Comparison of pore size distribution of ECC mixtures with FA and slag at 28 days	47
Figure 4.4 Crack width-time relations of overlay mixtures under restrained shrinkage	49
Figure 4.5 Load vs. deflection curves of pavement overlay mixtures with different thicknesses after four point bending test at the age of 28 days.....	52
Figure 4.6 Crack propagations of layered composite beams after four point bending test.....	53

Figure 4.7 Load vs. deflection graph of pavement overlay mixtures after reflective cracking test at the age of 28 days.....57

Figure 4.8 Crack patterns at failure of overlay materials after reflective cracking test58

LIST OF TABLES

	Page
Table 2.1 Typical mixture proportions of concrete and ECCs.....	9
Table 3.1 Chemical and physical properties of Portland cement, fly ash, slag and micro-silica.....	24
Table 3.2 Mechanic and Geometric Properties of PVA Fibers.....	29
Table 3.3 Mixture proportions and main properties	30
Table 4.1 Compressive Strength of overlay materials	42
Table 4.2 Flexural properties of overlay materials	43
Table 4.3 Restrained shrinkage crack characterization of overlay mixtures.....	48
Table 4.4 Flexural strengths of F_ECC, S_ECC and MSC composite beams after four point bending test	50
Table 4.5 Maximum flexural loads of composite beams after reflective cracking test	55

LIST OF SYMBOLS/ABBREVIATIONS

AEA	Air entraining admixture
AWI	Aggregate wear index
d_f	Fiber diameter
ECC	Engineered cementitious composites
E_m	Elastic modulus of the mortar matrix
$e^{f\phi}$	Accounts for the changes in bridging force for fibers crossing at an inclined angle to the crack plane
f	Snubbing coefficient
F_ECC	Fly ash with Engineered Cementitious composites
FA	Fly ash
FRC	Fiber reinforced concrete
HPFRCC	High performance fiber reinforced cementitious composites
HRWR	High range water reducing admixture
J'_b	Complimentary energy
J_{tip}	Fracture energy of the mortar matrix
K_m	Fracture toughness of the mortar matrix
L_f	Fiber length
LVDT	Linear variable displacement transducer
MAS	Maximum aggregate size

MIP	Mercury intrusion porosimetry
MOR	Modulus of rupture
MSC	Micro silica concrete
$p(z)$	Centroidal distance from the crack plane
$P(\delta)$	Pullout load versus displacement relation of a single fiber aligned normal to the crack plane
$p(\phi)$	Probability density functions of the fiber orientation angle
PC	Portland cement
PE	Polyethylene
PVA	Polyvinyl-alcohol fibers
RH	Relative humidity
S	Ground granulated blast furnace slag
S_ECC	Slag with Engineered Cementitious composites
SEM	Scanning electron microscope
SUBC	Substrate concrete
V_f	Fiber volume fraction
W/CM	Water to cementitious material ratio
z	Centroidal distance of a fiber from the crack plane
δ_0	Crack opening
ϕ	Orientation angle of the fiber
σ_0	Maximum crack bridging stress
σ_{fc}	First cracking strength of the mortar matrix

CHAPTER I

INTRODUCTION

1.1 General

The use of rigid concrete pavements has become increasingly popular for places subjected to moderate and heavy traffic loads, such as bridge deck, highway and airport pavements and industrial floor rehabilitation, due to their high load carrying capacity and low maintenance requirement compared to flexible asphalt concrete pavements (Zhang and Li, 2002). Several hundred thousand kilometers of rigid concrete pavements had been built around the world in the past decades. At present, most of those concrete pavements are either approaching the end of their design lives or in need of repair (Emmanuel, et al., 1998). For pavements subjected to moderate and heavy traffic loads, the most common rehabilitating method is to place an overlay on the existing pavement. Asphalt concrete and Portland cement concrete are the most prevalent materials to form the overlays, which provide protection to the pavement structure, reduce the rate of pavement deterioration, provide a smooth riding surface and strengthen the existing pavement, thus extending the pavement service life (Emmanuel et al., 1998). Depending on the application, traffic requirements and condition of the pavement structure, an overlay may be as thin as 50 mm (ultra-thin) or as thick as 150 mm or more (Fwa and Paramasivam, 1990; Risser et al., 1993; Cable and Hart, 1998). Although, this is a good solution for pavement improvement, some problems can still appear such as reflective cracking, which occurs when the existing cracks in the underlying pavements reflect into the newly constructed overlay under shrinkage and/or temperature change, and traffic loads. Cracking in overlay slabs reduces the load carrying capacity, allows water and other aggressive agents, such as deicing salts, to go through the cover layer to come into contact with the reinforcement bars, leading to corrosion and rupture. Cracks in the top layer of a pavement may also cause pumping of soil particles through the cracks, thus reducing the soil load bearing capacity (Sikdar et al., 1999).

Also, severely spalled and wide cracks will increase the roughness of the pavement and reduce its serviceability to the driver and also result in discomfort for users, finally generally leading to service termination. In addition to the reflective cracking, due to the difference in deformation behavior between new constructed overlay and old pavement under mechanical and environmental loading, a certain delamination along the interface of overlay and old pavement starting from the existing cracks will take place (Zhang and Li, 2002). Therefore, the prevention of overlay delamination and reflective cracking in overlaid slabs are crucial.

The quasi-brittle nature of plain concrete under mechanical and environmental loading is one of its major obstacles to the successful overlay applications. With the brittle nature of concrete, cracks can propagate rapidly to result in failure at a low ultimate strain (around 0.01% ultimate tensile strain) without warning. During the last decade concrete technology has been undergoing rapid development. The effort to modify the brittle behavior of plain cementitious materials has resulted in modern concepts of high performance fiber reinforced cementitious composites (HPFRCC) that exhibit pseudo-ductile behavior under uniaxial tension load. In plain concrete, after the first crack there is no load carrying capacity. In conventional fiber reinforced cementitious composites, matrix cracking is followed by a reduction in load carrying capacity known as residual strength. For HPFRCC, after the formation of the first through crack, the fibers themselves are able to carry the additional load. On further loading, multiple micro-cracks will form along the member, leading to a significant increase in strain. The tensile stress-strain curve will hence exhibit a post-cracking hardening branch similar to that of ductile materials. Engineered Cementitious Composites (ECC) is a special class of HPFRCC with extremely high tensile ductility. It is designed to strain harden in tension based on micromechanical principles, which allows optimization of the composite for high performance represented by extreme ductility while minimizing the amount of reinforcing fibers, typically less than 2% by volume (Li, 1998; Li, 2003 and Li et al., 2001). The most distinctive characteristic separating ECC from conventional concrete and fiber reinforced concrete (FRC) is an ultimate tensile strain capacity between 2 to 4%, depending on the specific ECC mixture. Along with tensile ductility, the unique crack development within ECC is critical to its durability. Different from ordinary concrete and most fiber reinforced concretes, ECC exhibits self-controlled crack

widths under increasing load. Even at large imposed deformation, crack widths of ECC remain small, less than 100 μm . With intrinsically tight crack width and high tensile ductility, ECC represents a new concrete material that offers a significant potential to naturally resolving the durability problem of concrete structures.

ECC promises to be used in a wide variety of civil engineering applications, as summarized in Japan Concrete Institute (JCI, 2002) and by Kunieda and Rokugo (2006). One of the most promising areas of application of this material is in the repair layer over an existing concrete substrate (Zhang and Li, 2002; Lim and Li, 1997; Kamada and Li, 2000). Experimental testing of ECC overlays reveals significant improvements in load-carrying capacity and system ductility compared to concrete or steel fiber reinforced concrete overlays (Qian, 2007). Through a unique “kinking-and-trapping” mechanism, the material’s ductility effectively prevents substrate cracks from reflecting through an ECC overlay. It was also shown that the common failure phenomenon of spalling or delamination in repaired concrete systems were eliminated with the use of ECC. Instead, microcracks originated from the tips of cracks on the ECC/concrete interface, kinked into and subsequently were arrested in the ECC material. Therefore, the surface crack width and interface delamination can be both minimized with the use of ECC. In addition, reflective cracking can be suppressed when ECC is used as the repair material (Zhang and Li, 2002).

1.2 Research Objectives and Scope

The current high cost of ECC may not justify their use, despite the lower life cycle costs achieved due to reduced maintenance requirements (Kendall et al., 2008 and Zhang et al., 2008). To facilitate the extended use of ECC in pavement construction (especially in developing countries), it is necessary to optimize the overlay thickness in order to obtain optimum performance at lowest possible cost. This is one of the main objectives of the current study. Regarding the overlay materials, the type of supplementary cementitious material used in ECC production was varied to control its ductility and strength. Thus, two different mixtures of ECC with fly ash and ground granulated blast furnace slag were used for the comparison of overlay performances. Layered ECC/concrete beams will be cast with three different ECC

layer thicknesses, namely 25, 35 and 50 mm. After measuring the basic mechanical properties of monolithic overlay specimens (compressive strength, flexural strength, drying and restrained shrinkage), layered ECC_concrete beam in which a layer of ECC is applied beneath a layer of substrate concrete under four point-bending tests were carried out to investigate the reflective cracking and flexural performances. The influences of ECC's strength and ductility, and layer thickness on the strength and ductility of the layered beam are discussed in experimental aspects. During the experimental study, microsilica concrete, one of the most commonly used type of overlay mixtures, was also cast and tested as control overlay materials.

This thesis is organized into five chapters as follows: Chapter 1 describes introduction for the research, objectives of the research, and scope of the work. In Chapter 2, (i) Proposed material solution for sustainable rigid pavement overlay (ii) Background of Engineered Cementitious Composites (ECC) (iii) Mechanical and environmental performance in pavement and cost of ECC are discussed in detail. In Chapter 3, experimental program, material properties and tests applied on the specimens are discussed. The results of the experimental studies are presented and discussed in Chapter 4. The conclusions of the research are presented in Chapter 5.

CHAPTER II

LITERATURE REVIEW AND BACKGROUND

2.1 Introduction

Around the world, the transportation systems of roadway are the most commonly used, maintained, and visible public modalities. For instance, in the year 2006, drivers in America drove about 3.0 trillion miles in vehicles across about 4 million miles of the public roadways in America (RITA, 2008). As there is a small controversy about the necessity to spread and preserve the systems of roadway infrastructure around the world in order to countenance economic growth in growing countries and persisted comfort in developed countries, the running trends of unsustainable material production, roadway building, operation, spoilage, frequent repairs, and destruction are appalling. Concrete pavements with non-renewable material production start with the production of Portland cement. More than 5 % of global anthropogenic greenhouse emissions (Battelle Group, 2002) are due to the mining, calcining, and grinding of Portland cements, which is very important reason for the global climate change. After first construction, inadequate maintenance of concrete pavements can be a reason for deterioration and related to repair needs. In 2009, American society of civil engineers introduced C and D grades to America's bridges and roads (American Society of Civil Engineers, 2009). Repeating cycles of short-term repair scenarios is due to this deteriorated state, and this leads to increase the repair materials and fuel consumption. The pavement systems sustainability also issues to the vehicles traveling over the pavement beside to material consumption. The traffic of automobiles and trucks produces 34% of our anthropogenic greenhouse emissions (RITA, 2008). Related to every building and maintenance event, overcrowding traffic increases fuel consumption and emissions. Furthermore emissions from traffic increase because the roughness of the pavement increases, during the service life. This exceptional case implicates an important piece of unsustainable state of technologies of concrete pavement.

Funding preliminaries for instance in the American Recovery and Reinvestment Act in the United States for increased maintenance and repairing is significantly needed to maintain the infrastructure in difficult condition, bigger maintenance will not be a solution to the great sustainability alters facing concrete pavements systems. A more basic solution for the concrete pavements, reinforced and unreinforced, is essential and it is closed to the material and system impacts that were described before. The problem is the durability of the concrete materials, even though it is economical and simple to construct. Many modes have been considered to develop durability of the concrete, like using high strength of concrete, concrete admixtures, epoxy coated reinforced, etc. But several solutions have conducted the attendant shortfall of concrete since its brittleness which cracks due to mechanical and environmental loads. The cracks are the main reason for corrosion and durability problems, leading to oxidation of the steel reinforcement, concrete faulting and pavement failure. In order to solve the problem as much as possible in concrete pavement sustainability challenges, a basic solution lowering the concrete brittleness is proposed.

2.2 Proposed Material Solution for Sustainable Pavement Overlay

An ideal overlay material, therefore, would be volumetrically stable, i.e. it would undergo neither shrinkage nor expansion once installed, and would display compatible modulus of elasticity, strength, creep, shrinkage, thermal expansion, permeability and electrochemical characteristics to the substrate. Unfortunately, despite the best efforts of product formulators such products do not appear to exist. Thus, the best that can be hoped for are overlay materials that have a suitable mechanical properties and sufficiently low volume change capacity that they neither shrink nor expand to the extent that they crack, or impose sufficient interfacial shear stress (or direct tensile stress) to cause bond failure.

During the last decade concrete technology has been undergoing rapid development. The effort to modify the brittle behavior of plain cement materials such as cement pastes, mortars and concretes has resulted in modern concepts of high performance fiber reinforced cementitious composites (HPFRCC) that exhibit ductile behavior under uniaxial tension load. In plain concrete, after the crack there is no load carrying capacity (Figure 2.1). In conventional fiber reinforced cementitious

composites, matrix cracking is followed by a reduction in load carrying capacity known as residual strength (lower curve in Figure 2.1). For HPFRCC, after the formation of the first through crack, the fibers themselves are able to carry additional load. On further loading, multiple micro cracks with crack width less than 100 μm will form along the member, leading to a significant increase in strain. The tensile stress-strain curve will hence exhibit a post-cracking hardening branch similar to that of ductile materials, such as aluminium (upper curves in Figure 2.1).

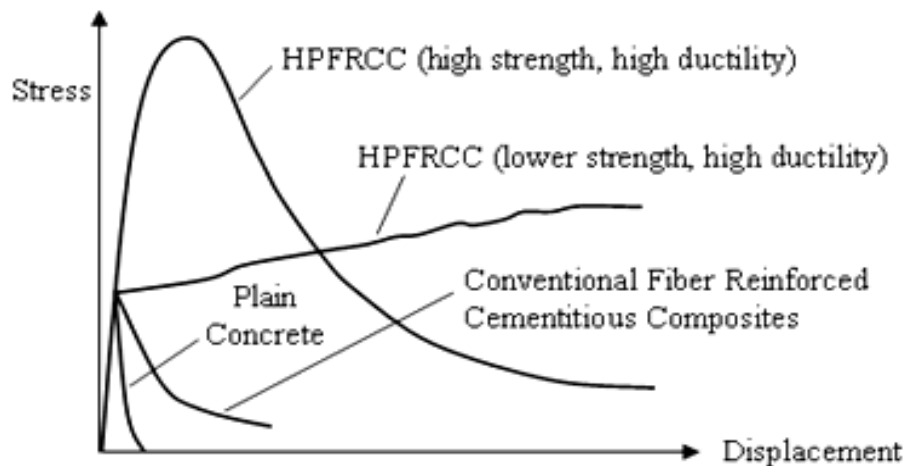


Figure 2.1 Tensile behavior of plain and fiber reinforced cementitious materials

The quantitative criterion for the achievement of ductility (inelastic straining), in terms of various material and geometric parameters (such as properties of fiber, matrix [composite without fiber], fiber-matrix interface, fiber geometry and volume fraction, etc.), was proposed by Li and Leung (1992) and further developed by Li (1993), and Kanda and Li (1999). With proper selection of parameters to fulfill the criterion, ductile composites with different strengths can be made with fiber volume from 1.5% to 5%. The actual ‘ductility’ of the HPFRCC, which can be defined as the strain at maximum tensile stress, depends on the effectiveness of fibers in transferring stress back into the matrix (which in turn depends on the microstructural parameters) as well as the toughness of the matrix itself (Li, 1997). Normally, the higher the matrix toughness, the lower will be the ductility achieved with a certain fiber volume fraction. Depending on the particular application, the material design can be varied to produce an optimal tensile stress vs. strain relation that satisfies the strength and ductility requirements. In the literature, HPFRCC’s have been given

different names by various researchers. These include Rossi and Parant (2005), Alaei and Karihaloo (2003) and hybrid fiber composites (Markovic, 2004), which are the high strength composites with relatively low ductility, as well as HPFRCC (Li, 1993), a highly ductile HPFRCC with moderate fiber volume (tensile failure occurs at 2-5% strain – 200-500 times that of conventional concrete or fiber reinforced concrete) with relatively low strength. This type of HPFRCC is also called as Engineered Cementitious Composites (ECC). After this section of the thesis, literature review is basically based on the studies related with ECC.

In elastic straining in the form of micro-crack damage has been demonstrated in ECC. Moreover, the self-healing of cracks becomes prominent when crack width is small. If durability, and eventually sustainability are important goals, current construction practice and the codes of recommended practice must undergo a paradigm shift to achieve concrete structures that have tight cracks or are ‘crack-free’ in preference to high strength. The formation of cracks coupled with a lack of crack width control in brittle concrete are primarily responsible for distresses that can dramatically reduce the long-term durability performance of concrete. While it is unrealistic to imagine the complete suppression of cracking in concrete, the ability to use robust self-healing functionality as an autogenous mechanism in areas with tight cracks may lead to the realization of such virtually ‘crack free’ concrete. In 2002, the Concrete Research and Education Foundation also listed such robust self-healing concretes second in its list of ‘high priority research topics’ for the concrete industry (CREFSDC, 2002). Self-healing is generally attributed to the hydration of previously unhydrated cementitious material, calcite formation, expansion of the concrete in the crack flanks, crystallization and closing of cracks by solid matter in the water (Ramm and Bischoff, 1998). Self-healing of cracks can only be taken into account when crack width is small (generally less than about 150 μm). Self-healed cracks or very tight cracks (less than 0.1 mm) do not pose a durability problem in concrete structures (Sahmaran et al., 2007; Yang et al., 2009).

The ductile behavior and self-healing characteristic of ECC is associated with many other desirable properties for overlay applications. These include (i) high energy absorption, impact resistance and tensile ductility (high in elastic strain), (ii) ability to redistribute localized stresses, thus reducing the sensitivity of the material to stress

concentrations, (iii) high deformability, passing ability, and resistance to segregation to secure complete filling of complex formwork and ease of production including self-consolidation casting and shotcreting (iv) high shear strength, (v) high bond strength to steel reinforcement and substrate concrete (high delamination resistance), and (vi) capability to control the opening of cracks, and hence preventing the resulting increase of transport properties that would lead to durability problems. However, three major limitations of ECC are the high cost, environmental issues and high shrinkage of the material. The cost is high because fibers are much more expensive than the basic components of conventional concrete. Currently, poly-vinyl alcohol (PVA), polyethylene (PE), and micro-steel fibers are the most successfully used fibers in the production of ECC. Compared with conventional concrete, HPRCC materials contain considerably higher cement content, typically two to three times higher. Table 2.1 shows the mixture proportions of typical PE_ECC (Li, 1997) and PVA_ECC (Li et al., 2002), along with conventional structural concrete.

Table 2.1 Typical mixture proportions of concrete and ECCs

Material (kg/m³)	PVA-ECC	PE-ECC	Conventional Concrete
Portland Cement	832	1205	390
Water	366	314	166
Aggregates	832	603	1717
Fiber	26	17	-
Superplasticizer	17	12	2

The high cement content in ECCs is a consequence of rheology control for easy fiber dispersion and, more essentially, matrix toughness control for strain-hardening behavior. To achieve high ductility (strain-hardening), matrix fracture toughness has to be limited such that multiple cracking could occur before reaching maximum fiber bridging stress. Large aggregates are hence eliminated in the mixture, resulting in a higher cement content compared with normal concrete. In fact, ECC materials use cement paste or mortar with fine sand as a matrix, and typically have cement content at 800 to 1200 kg/m³. High cement usage results in undesirably high hydration heat as well as high material cost and drying shrinkage. In addition, such matrixes

apparently compromise sustainability performance of the material, as cement production is responsible for 7% of global greenhouse gas emissions generated by human activities, (Malhotra, 1998; Mehta, 1998) and significant levels of nitrogen oxides, particulate matter, and other pollutants. Moreover, ECC could generate relatively large shrinkage strain compared to conventional concrete due to relatively high cement content, low water-cement ratio and lack of coarse aggregate, thus increasing cracking potential of the concrete. However, the presence of fibers can control the crack width such that deterioration is not an issue.

2.3. Engineered Cementitious Composites (ECC)

2.3.1 Background of Engineered Cementitious Composites

As a new class of HPFRCC materials, Engineered Cementitious Composites (ECC) is a ductile fiber reinforced cementitious composite micromechanically designed to achieve high damage tolerance under severe loading and high durability under normal service conditions (Li, 1998; Li et al., 2001; Li, 2003). The most distinctive characteristic separating ECC from conventional concrete and fiber reinforced concrete (FRC) is an ultimate tensile strain capacity between 3 to 5%, depending on the specific ECC mixture. This strain capacity is realized through the formation of many closely spaced microcracks, allowing for a strain capacity over 300 times that of normal concrete. These cracks, which carry increasing load after formation, allow the material to exhibit strain hardening, similar to many ductile metals.

While the components of ECC may be similar to FRC, the distinctive ECC characteristic of strain hardening through microcracking is achieved through micromechanical tailoring of the components (i.e. cement, aggregate, and fibers) (Li, 1998; Lin et al., 1999; Li et al., 2001; Li, 2003), along with control of the interfacial properties between components. Fracture properties of the cementitious matrix are carefully controlled through mix proportions. Fiber properties, such as strength, modulus of elasticity, and aspect ratio have been customized for use in ECC. The interfacial properties between fiber and matrix have also been optimized in cooperation with the manufacturer for use in this material.

While most HPFRCCs rely on a high fiber volume to achieve high performance, ECC uses moderate amounts, typically 2% by volume, of short, discontinuous fiber. This low fiber volume, along with the common components, allows flexibility in construction execution. To date, ECC materials have been engineered for self-consolidation casting (Kong et al., 2003), extrusion (Stang and Li, 1999), shotcreting (Kim et al., 2003), and conventional mixing in a gravity mixer or conventional mixing truck (Lepech and Li, 2007).

Figure 2.2 shows a typical uniaxial tensile stress-strain curve of ECC material containing 2% poly-vinyl-alcohol (PVA) fiber (Weimann and Li, 2003b). The characteristic strain-hardening behavior after first cracking is accompanied by multiple microcracking. The crack width development during inelastic straining is also shown in Figure 2.2. Even at ultimate load, the crack width remains smaller than 80 μm . This tight crack width is self-controlled and, whether the composite is used in combination with conventional reinforcement or not, it is a material characteristic independent of rebar reinforcement ratio.

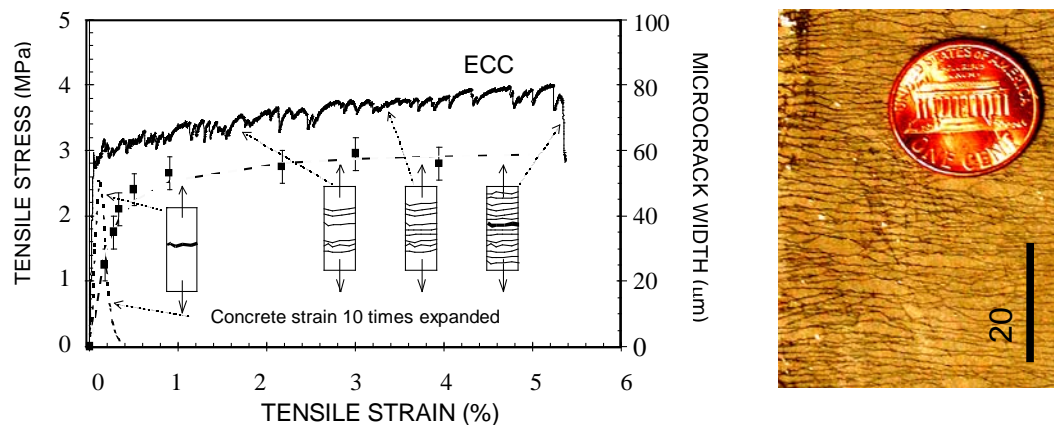


Figure 2.2 Typical tensile stress-strain curve and crack width development of ECC (Weimann and Li, 2003b)

In contrast, normal concrete and fiber reinforced concrete rely on steel reinforcement for crack width control. Under severe bending loads, an ECC beam deforms similar to a ductile metal plate through plastic deformation (Figure 2.3). In compression, ECC materials exhibit compressive strengths similar to high strength concrete (e.g. greater than 60 MPa) (Lepech and Li, 2007).

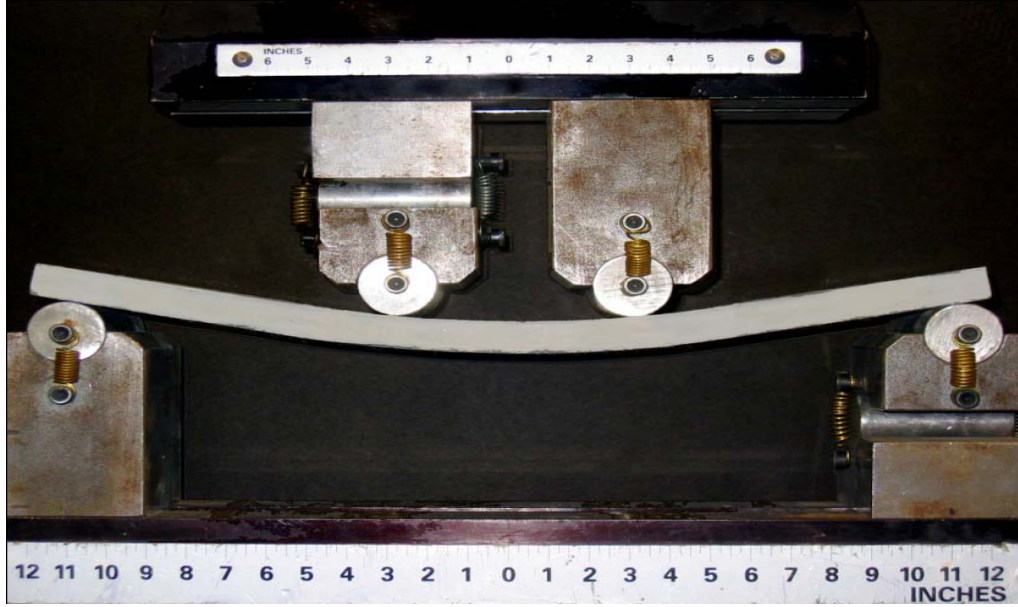


Figure 2.3 Response of ECC under flexural loading

2.3.2 Design of Engineered Cementitious Composites

The first priority when designing ECC material is to ensure the formation of multiple cracks and strain-hardening behavior under load. This allows large deformations to be distributed over multiple micro-cracks. The basis of multiple micro-cracking and strain hardening within ECC is the propagation of steady state cracks which were first characterized by Marshall and Cox (1988), and extended to fiber reinforced cementitious composites by Li and Leung (1992) and Lin et al. (1999). By forming steady state “flat cracks” which maintain a constant crack width while propagating, rather than Griffith-type cracks which widen during propagation as in typical tension-softening fiber reinforced cementitious materials, ECC material exhibits multiple micro-cracks which saturate the specimen while undergoing strain-hardening during extreme tensile deformation. The formation of multiple steady state cracking is governed by the bridging stress versus crack width opening relation along with the cracking toughness of the mortar matrix. To achieve this phenomenon the inequality shown in Equation-2.1 must be satisfied.

$$J'_b = \sigma_0 \delta_0 - \int_0^{\delta_0} \sigma(\delta) d\delta \geq J_{tip} \approx \frac{K_m^2}{E_m} \quad (2.1)$$

Where J'_b is the complimentary energy shown in Figure 2.4, σ_0 and δ_0 are the maximum crack bridging stress and corresponding crack opening, J_{tip} is the fracture energy of the mortar matrix, K_m is the fracture toughness of the mortar matrix, and E_m is the elastic modulus of the mortar matrix. In addition to the fracture energy criterion, a strength criterion expressed in Equation-2.2 must be satisfied.

$$\sigma_0 > \sigma_{fc} \quad (2.2)$$

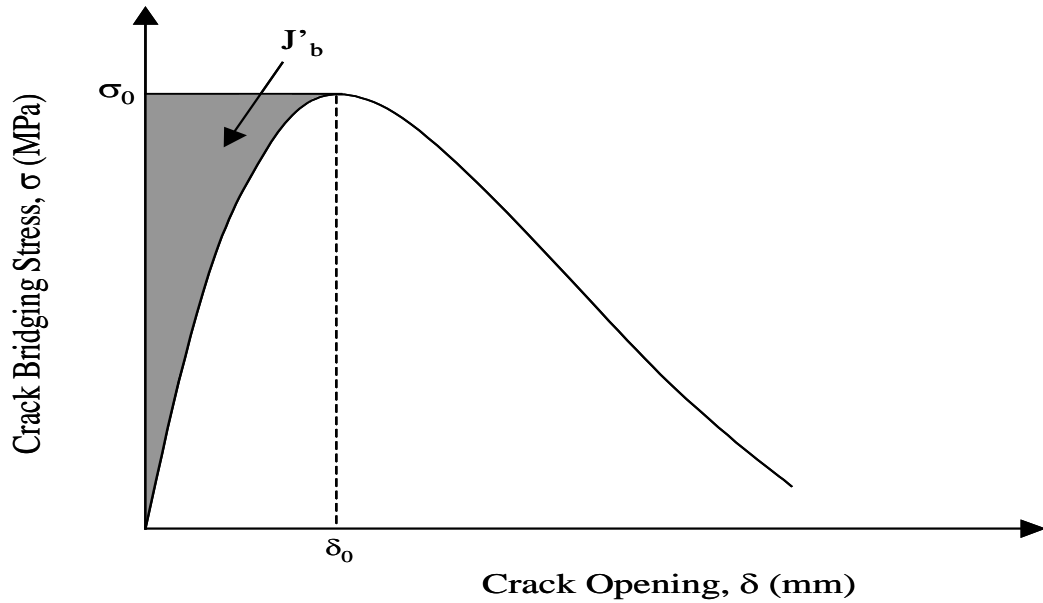


Figure 2.4 Crack bridging stress versus crack opening relation

Where, σ_0 is the maximum crack bridging stress and σ_{fc} is the first cracking strength of the mortar matrix. For saturated multiple cracking, Wang and Li (2004) found that Equation-2.2 must be satisfied at each potential crack plane, where σ_{fc} is understood as the cracking stress on that crack plane.

Once an ECC mixture is selected which sufficiently meets the two above criteria, the formation of multiple steady state cracks, and strain-hardening performance, can be realized. However, in addition to forming these cracks, the material must also be designed to exhibit crack widths below the 100 μm threshold limit. This can be achieved through tailoring of the crack bridging versus crack opening relation referenced in Equation-2.1. The maximum steady state crack width exhibited during ECC multiple cracking can be assumed to be δ_0 , the crack width corresponding to the maximum crack bridging stress, σ_0 , as shown in Figure 2.4. If the crack width were

to grow beyond δ_0 , the crack bridging stress would begin to fall, in which case the crack would localize and multiple crack formation would cease. By keeping δ_0 below the 100 μm threshold, the ECC material can exhibit multiple cracking and strain hardening performance.

Lin et al. (1999) proposed the formulation of the crack bridging stress versus opening relationship based on summing the bridging force contribution of fibers that cross a given crack plane. This relation is expressed in Equation-2.3.

$$\sigma(\delta) = \frac{4V_f}{\pi d_f^2} \int_{\phi=0}^{\pi/2} \left(\int_{z=0}^{(L_f/2)\cos\phi} P(\delta) e^{f\phi} p(\phi) p(z) dz \right) d\phi \quad (2.3)$$

where V_f is the fiber volume fraction, d_f is the fiber diameter, ϕ is the orientation angle of the fiber, L_f is the fiber length, z is the centroidal distance of a fiber from the crack plane, f is a snubbing coefficient, and $p(\phi)$ and $p(z)$ are probability density functions of the fiber orientation angle and centroidal distance from the crack plane, respectively. $P(\delta)$ is the pullout load versus displacement relation of a single fiber aligned normal to the crack plane, also described in Lin et al. (1999). The factor $e^{f\phi}$ accounts for the changes in bridging force for fibers crossing at an inclined angle to the crack plane.

Using these basic micromechanical models to tailor the ECC material, a composite can be designed to undergo large deformations, up to several percent, without sacrificing low permeability due to large crack widths. The application of material design procedures, such as those outlined above, allow materials engineers to carefully match material characteristics to specific structural demands, such as strain capacity and low permeability.

2.4 Use of ECC as an Overlay Material

The most usual deformations like spalling and delamination of repair parts in rehabilitated infrastructures can be prevented by trapping mechanism of the ECC overlay system. In addition, we can expect high ultimate strength and large deflection capacity with large amount of energy absorption capacity. The ultimate

failure method has been shifted from one related to interface crack extension to one related to the flexural repair material strength. The sudden development in the strength, deflection, energy absorption capacity and ultimate failure mode is not possible without trapping mechanism based on interface fracture mechanics and ECC material design. Also this overlay system can give a very low water permeability in rehabilitated infrastructures.

ECC overlays are designed to improve the durability in two ways, first, ‘greener’ ECC materials work together with industrial remaining materials like fly ash, ground granulated blast, furnace slag (GGBFS), and waste foundry sands and carbon residue in order to decrease the environmental effects of material production. Green material design is carefully guided by fundamental micromechanics in order to sustain pseudo-strain hardening material behavior under uniaxial tension. This ductile behavior is critical to the second mechanism for sustainability enhancement. Through a different storm, premature overlay failure, cracking is eliminated by ECC ductility very well. So life-cycle maintenance reduces and durability increases. Green material and overlay design approaches are verified by experimental and theoretical analysis. Without decreasing critical mechanical performance characteristics, over 70% of ECC virgin parts have been replaced with incorporating industrial wastes. The combination of green raw materials, a 50% reduction in overlay thickness, and a doubling of service life as compared to concrete overlays, leads to significant sustainability improvements have been achieved.

2.4.1 Mechanical and Environmental Performance of ECC in Pavement Applications

To evaluate the performance of ECC under typical transportation-related mechanical and environmental loads, durability tests and long-term performance studies on ECC materials have been conducted by the other researchers. These tests include restrained shrinkage tests, fatigue and bonding tests, freeze thaw exposure, wearing/abrasion tests, and accelerated environmental tests. Additionally, the long-term strain capacity and early age strength development of ECC have been investigated. These studies confirm that ECC will successfully perform as a rigid pavement overlay material for highway applications.

2.4.1.1 Shrinkage

To examine the restrained shrinkage behavior of ECC, ring tests (AASHTO PP-34) were carried out for both ECC and normal Portland cement concrete. Due to the high cement content of ECC, significantly higher free shrinkage deformation is exhibited, compared to normal concrete (Weimann and Li, 2003a). However, restrained shrinkage tests show that although hygral deformation may be higher, crack widths in ECC remain below 50 μm (50% relative humidity, RH, for 100 days), compared to concrete crack widths of approximately 1 mm (Figure 2.5). This is achieved through the microcracking of ECC, allowing the shrinkage deformation to be distributed over a large number of small cracks, while all shrinkage deformation in concrete localizes at a single crack. Further, the formation of shrinkage cracks at ECC/concrete interfaces is prevented by lower interfacial stresses due to the large deformability of ECC.

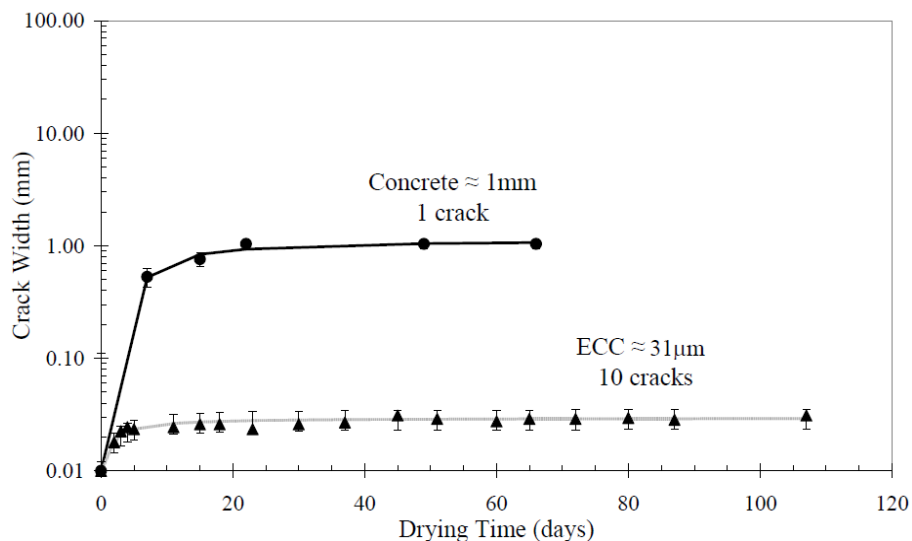


Figure 2.5 Crack Width Development as a Function of Drying Time (RH=50%) (Weimann and Li, 2003a).

2.4.1.2 Fatigue Testing and Overlay Bond Characteristics

The performance of ECC has been investigated in high fatigue scenarios, such as rigid pavement overlay rehabilitation. In these overlay applications, reflective cracking through the new overlay is of greatest concern. Existing cracks and locally reduced load capacity in the substrate pavement can result in flexural fatigue within

the overlay structure. To evaluate ECC performance as a rigid pavement overlay material, both ECC/concrete and concrete/concrete overlay specimens were tested in flexural fatigue (Zhang and Li, 2002). Test results show that the load carrying capacity of ECC/concrete overlay specimens was double that of concrete/concrete overlay specimens, the deformability of ECC/concrete specimens was significantly higher, and the fatigue life was extended by several orders of magnitude. Further, the microcracking deformation mechanism of ECC effectively eliminated reflective cracking. Similar advantages in the fatigue resistance of ECC have also been found in comparison to polymer cement mortars (Suthiwarapirak et al., 2002). Fatigue resistance of ECC for repair of viaducts subjected to train loading was studied by Inaguma et al. (2005). In fatigue-prone concrete infrastructure, the application of ECC materials may be able to significantly lengthen service-life, reduce maintenance events, and life cycle costs.

In addition to fatigue performance and crack resistance, the bond characteristics of ECC/concrete repairs were investigated. Using ECC as an overlay material, the delamination and spall processes, typically seen in many concrete/concrete repairs, were eliminated. Through a unique kinking-and-trapping crack formation process, both the load capacity and energy absorption of the ECC/concrete overlay was increased over concrete/concrete system. In this mechanism, cracks propagate slightly along the bonding interface but are then directed into the ECC overlay and immediately arrested by the high ECC toughness (34 kJ/m^2) (Maalej et al., 1995). This kinking-and-trapping process repeats until the ECC ultimately fails in flexure, unrelated to interfacial debonding. Additionally, the influence of surface preparation on bonding was investigated. Tests show that regardless of a smooth or roughened interface, the bond performance of an ECC/concrete overlay is superior to that of a concrete/concrete overlay (Li, 2003b). The bond characteristics of ECC/concrete repair applications prove to be far better than current concrete/concrete repair techniques.

2.4.1.3 Freeze-Thaw and Salt Scaling Resistance

It is well known that the cyclical freeze-thaw cycles and the use of de-icing salts during winter are two of the major causes of rapid degradation in concrete

pavements, bridge decks, parking structures, and similar structures. ECC used for this kind of structures must be resistant to cyclical freezing and thawing, and the effects of de-icing agents. It is known that a proper air-void system is generally needed in normal concrete to avoid internal cracking due to freeze-thaw cycles and scaling due to freezing in the presence of deicer salts.

Durability of non-air-entrained ECC specimens was tested by exposure to cycles of freezing thawing testing, in accordance with ASTM C666 (Li et al., 2003). Non-air-entrained concrete specimens were also tested as reference specimens. Non-air-entrained specimens were used as control since no air entrainment was added to the ECC mixtures. After 110 cycles, the concrete specimens had severely deteriorated, requiring removal from the freeze-thaw machine, as mandated by the testing standard. However, all ECC specimens survived the test duration of 300 cycles with no degradation of dynamic modulus. Figure 2.6 shows the typical surface condition of the after 300 freeze-thaw cycles and fog room cured prismatic ECC specimens. This performance results in a durability factor of 10 for concrete compared to 100 for ECC, as computed according to ASTM C666 (1991). In uniaxial tension tests performed on wet cured and freeze-thaw exposed ECC tensile coupons at the same age, no significant drop in strain capacity was experienced after 300 cycles. Both wet cured and freeze thaw specimens exhibited a strain capacity of roughly 3%. Both wet cured and freeze thaw specimens exhibited a strain capacity of roughly 3%.

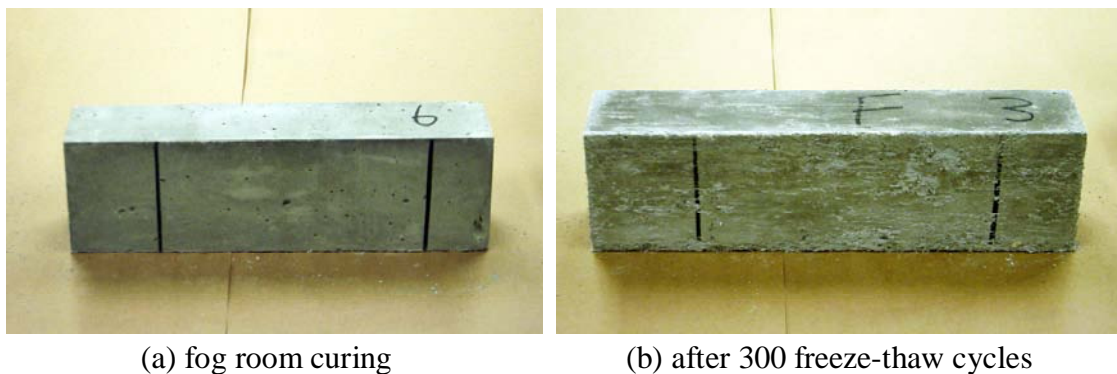


Figure 2.6 ECC specimen surface appearance after (a) normal curing and (b) freeze-thaw cycles

Numerous laboratory test data in accordance with ASTM C672 (2001) have indicated that air entrained concretes incorporating high volume fly ash often perform unsatisfactorily when exposed to freezing and thawing cycles in the

presence of de-icing salts. For the production of ECC, as much as two-thirds of the portland cement is substituted by fly ash. Due to the high volume fly ash content, it is important to test the performance of ECC exposed to freezing and thawing cycles in the presence of de-icing salt. Salt scaling resistance of non-air-entrained sound (uncracked) and mechanically pre-loaded (cracked) ECC specimens was evaluated by Şahmaran and Li in accordance with ASTM C672 (Şahmaran and Li, 2007). Non-air-entrained mortar specimens with and without fly ash were also tested as reference specimens. After 50 freeze-thaw cycles in the presence of de-icing salt, the surface condition visual rating and total mass of the scaling residue for ECC specimens, even those with high volume fly ash content, remain within acceptable limits of ASTM C672 (Figure 2.7). This level of durability holds true even for ECC specimens pre-loaded to high deformation levels and exhibiting extensive microcracking.

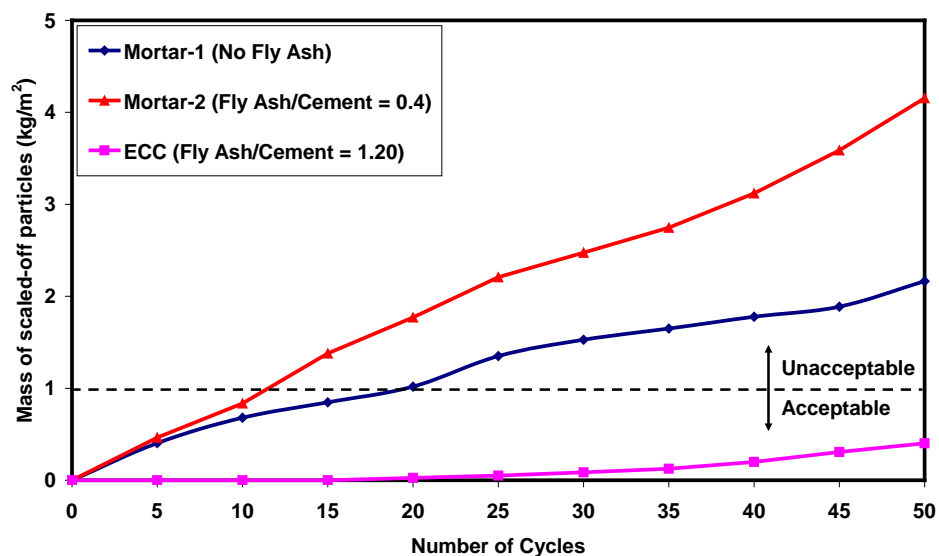


Figure 2.7 Mass of scaled-off particles versus number of freeze thaw cycles for virgin mortar and virgin ECC prisms in presence of de-icing salts (Şahmaran and Li, 2007).

In comparison, reference mortar specimens under identical testing conditions deteriorated severely. Moreover, the replacement of fly ash with cement in mortar further exacerbated deterioration due to freezing and thawing cycles in the presence of de-icing salt. In a separate test, both pre-loaded (cracked) and sound ECC coupon specimens were exposed to freeze-thaw cycles in the presence of de-icing salts for 25

and 50 cycles to compare residual tensile strength and ductility of reloaded ECC specimens. The reloaded specimens showed negligible loss of ductility, and retained the multiple micro-cracking behavior and tensile strain capacity of more than 3%. It was also discovered that micro-cracks due to mechanical loading will heal sufficiently under freezing and thawing cycles in the presence of salt solutions, restoring them to nearly the original stiffness. These results confirm that ECC, both sound and micro-cracked, remains durable despite exposure to freezing freeze-thaw cycles in the presence of de-icing salts.

2.4.1.4 Abrasion and Wear Testing

For pavement surface and bridge deck repairs, ECC must provide an adequate surface for driving and braking, while withstanding traffic abrasion. Specimens were cured for 28 days and subjected to both static friction testing and wear track testing according to Michigan Test Method 111 (2001). Initial friction forces between vehicle tires operating at 65 kph and the textured ECC specimens were determined using a Michigan Department of Transportation (MDOT) static friction tester. All static friction tests were conducted on a wet pavement surface. Following initial friction testing, ECC specimens were subjected to 4 million tire passes to simulate long term tire wear. After wearing, friction forces were again determined to assess deterioration or surface polishing during wearing. These final friction forces equate to an Aggregate Wear Index (AWI) used for long term evaluation of pavement wear. AWI values for the textured ECC samples tested range from 1.6 kN to 2.3 kN (Li et al., 2003). The established minimum AWI for Michigan trunkline road surfaces is 1.2 kN, significantly lower than all ECC surfaces tested, indicating its suitability for roadway surface repairs subject to heavy traffic volumes.

2.4.1.5 Early Age Strength

Roadway surface repair materials must exhibit rapid early age strength development for infrastructure applications. Obviously, the longer a material cures before achieving adequate strength to withstand service loads, the larger an impact the project will have on traffic congestion and delays. To determine the early age

strength development of ECC, a series of compressive cylinders (10 cm x 20 cm) were tested at various early ages. Tests were conducted up to an age of approximately 100 hours. Tests show that at 24 hours, ECC exhibits a compressive strength of 24 MPa, adequate for most repair applications. After another 5 hours of curing the strength has reached 28 MPa, a typical required concrete strength in reinforced concrete construction. The ultimate compressive strength of a typical ECC material is 60 MPa, well above most transportation needs. From these results, a curing time of one day is recommended for typical repair applications. While the use of hydration accelerators was not included in this study, a variety of acceleration techniques have successfully been used with ECC to achieve adequate compressive strengths after only hours.

2.4.1.6 Long Term Strain Capacity

To validate the long-term viability of ECC pavements, a series of tensile tests have been performed to determine long-term strain capacity. Due to the delicate balance of cement matrix, fiber, and matrix/fiber interface properties which must be maintained to achieve strain hardening, the strain capacity of ECC material changes during the maturing process. This is exhibited in a plot of ECC strain capacity versus age (Figure 2.8) (Li and Lepech, 2004).

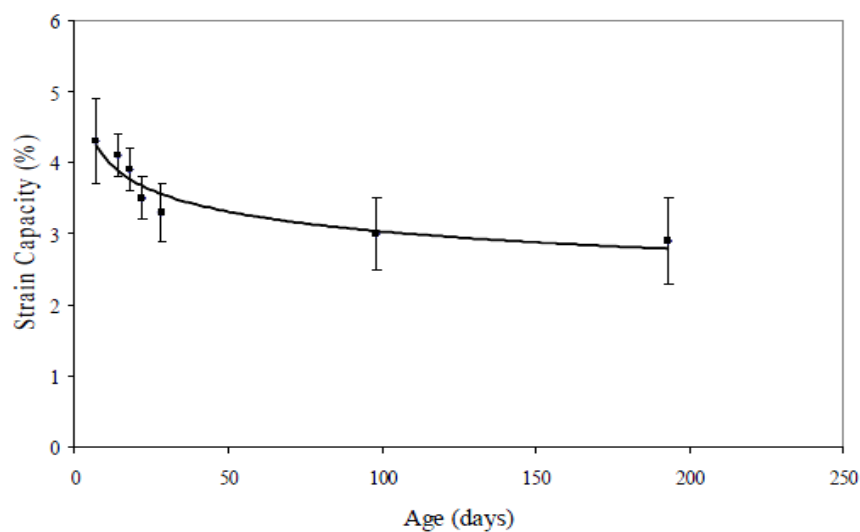


Figure 2.8 Tensile strain capacity development of ECC material (Li and Lepech, 2004).

Initially, strain capacity is very low due to the low strength of the matrix. For the ECC mix design shown, at roughly 10 days aging peak strain capacity is achieved due to an optimal balance of matrix, fiber, and matrix/fiber interface properties. As hydration continues, a slight imbalance occurs and remains throughout the life of the material resulting in a long-term strain capacity of 3% for ECC material. As mentioned before, this long term strain capacity data fits well with the strain capacity exhibited by freeze thaw and wet cured tensile specimens at 14 weeks. While long-term tests have only been carried out to 180 days, the long-term strain capacity has asymptotically reached approximately 3%.

2.4.1.7 Accelerated Weathering Tests

In contrast to freeze thaw tests which are designed to simulate temperature changes in winter conditions, hot water immersion tests were conducted to simulate the long term effects of hot and humid environments. To examine the effects of environmental exposure, hot water immersion was performed on individual fibers, single fibers embedded in ECC matrix, and composite ECC material specimens (Li et al., 2004). Specimens for both individual fiber pull-out and composite ECC material were cured for 28 days at room temperature prior to immersion in hot water at 60 °C for up to 26 weeks. After 26 weeks in hot water immersion, little change was seen in fiber properties such as fiber strength, fiber elastic modulus, and elongation. The tensile strain capacity of the ECC dropped from 4.5% at early age to 2.75% after 26 weeks of hot water immersion. While accelerated hot weather testing does result in lower strain capacity of ECC, the 2.75% strain capacity exhibited after 26 weeks remains over 250 times that of normal concrete.

2.4.2 Cost of ECC Materials

The funds required for up to date technology compared with present material is very essential to any transportation or infrastructure owner. With a price of about \$99/m³, normal Portland cement concrete is considered one of the simplest and the most economically useful materials used in designing of infrastructures. Anyway, just like we have discussed before, this material has a characterizing lifetime shortage, which

make it need more renewal at more duration costs. Highly strength concretes, which are commonly believed to have a longer lifetime than ordinary concrete, or traditional steel fiber reinforced concrete's price may rise to nearly \$199/m³. The recent price of PVA-ECC material is nearly \$349/m³. However, in the patch application, the price of the MDOT fixing materials is about \$539/m³. On the other hand, the price of ECC might appear higher in when compared to ordinary concrete, it is quite fewer than a lot of polymer concretes generally that are being used in repairing structures, or specific highly strength FRC, which might reach \$2000/m³- \$5000/m³ in price. As early noted, it is fundamental for the transportation society to look for basic methods to overcome inconvenient condition of the international infrastructures. Supported by a proof with initiatives, for example Michigan's "Preserve First", the requirement and resources for an enhanced transport infrastructure are found. A designer person must not look at precursors for fixing and renewing initially cost, and look for long lasting material, for instance ECC, that might cost a bit more than other commonly used material do. This highly performing material offers long lasting service life with decreased duration costs incorporated with repeated fixing, renewal, and displacing material. It is essential for transport plan makers and design experts to look to modern "brighter" material for the following generations to develop infrastructures.

CHAPTER III

EXPERIMENTAL PROGRAM

3.1 Materials

3.1.1 Portland Cement

The cement used in all mixtures was a normal Portland cement CEM I 42.5R (C), which correspond to ASTM Type I cement. It had a specific gravity of 3.06 and Blaine fineness of 325 m²/kg. Chemical composition and physical properties of cement are presented in Table 3.1. The morphological property of Portland cement obtained from SEM analysis is given in Figure 3.2

Table 3.1 Chemical and physical properties of Portland cement, fly ash, slag and micro-silica

Chemical Composition	Cement	Fly Ash	Slag	Micro-silica
CaO (%)	61.43	1.64	34.48	0.62
SiO ₂ (%)	20.77	56.22	38.40	91.96
Al ₂ O ₃ (%)	5.55	25.34	10.96	1.20
Fe ₂ O ₃ (%)	3.35	7.65	0.81	0.84
MgO (%)	2.49	1.80	7.14	1.02
SO ₃ (%)	2.49	0.32	1.48	0.12
K ₂ O (%)	0.77	1.88	0.86	1.16
Na ₂ O (%)	0.19	1.13	0.18	0.67
Loss of ignition (%)	2.20	2.10	3.00	1.86
SiO ₂ +Al ₂ O ₃ +Fe ₂ O ₃	29.37	89.21	50.17	94.00
Physical properties				
Specific gravity	3.06	2.31	2.79	0.60
Blaine fineness (m ² /kg)	325	290	425	-

The particle size distributions of cement, obtained by a laser scattering technique, is given in Figure 3.1.

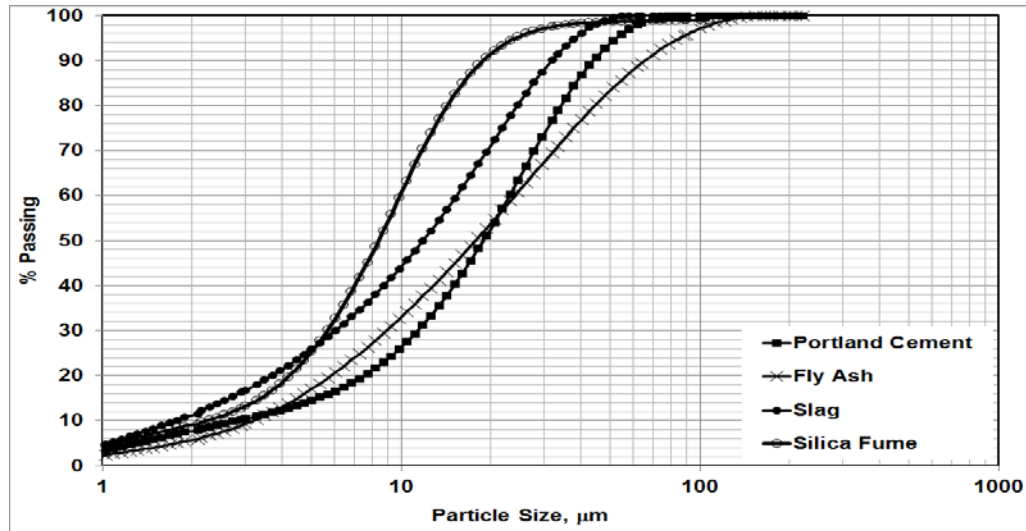


Figure 3.1 Particle size distributions of Portland cement, fly ash, slag and silica fume.

3.1.2 Mineral Admixtures

3.1.2.1 Fly Ash

Class-F fly ash (FA) conforming to ASTM C 618 (2003) requirements with a lime content of 1.64% obtained from Sugözü Thermal Power Plant was used. The chemical properties of FA are given in Table 3.1. The specific gravity and Blaine fineness of FA are 2.31 and 290 m²/kg, respectively. The particle size distribution of FA is provided in Figure 3.1. Figures 3.2 illustrate the particle morphology of FA. The scanning electron microscope (SEM) image showed that the particles of FA had significantly smooth spherical particles in comparison to slag.

3.1.2.2 Slag

Slag (S) was supplied from Iskenderun Iron–Steel Factory in Turkey. Its chemical oxide composition is given in Table 3.1. The specific gravity of slag was 2.79 g/cm³. The slag was ground granulated in Iskenderun Cement Factory to have a Blaine specific surface area about 425 m²/kg. According to ASTM C 989 (2009) hydraulic activity index, the slag used was classified as a category 80 slag. Particle size

distribution of slag obtained by using the laser diffraction is shown in the Figure 3.1. To identify morphological characteristics of slag, it was analyzed with SEM and the resulting photograph is presented in Figure 3.2.

3.1.2.3 Micro-silica

Micro-silica (MS), that was used for preparing micro-silica concrete (MSC) as an overlay, was supplied. Chemical composition and physical properties of micro-silica are presented in Table 3.1. Particle size distribution of micro-silica obtained by using the laser diffraction can be seen in Figure 3.1. The morphological property of micro silica obtained from SEM analysis is given in Figure 3.2. Micro-silica was used for preparing MSC, and the behavior of overlay system using MSC as a control was compared with the overlay system behavior using fly ash-ECC (F_ECC) and slag-ECC (S_ECC) as potential overlay materials. Chemical and physical properties of micro-silica (silica fume) are also presented in Table 3.1.

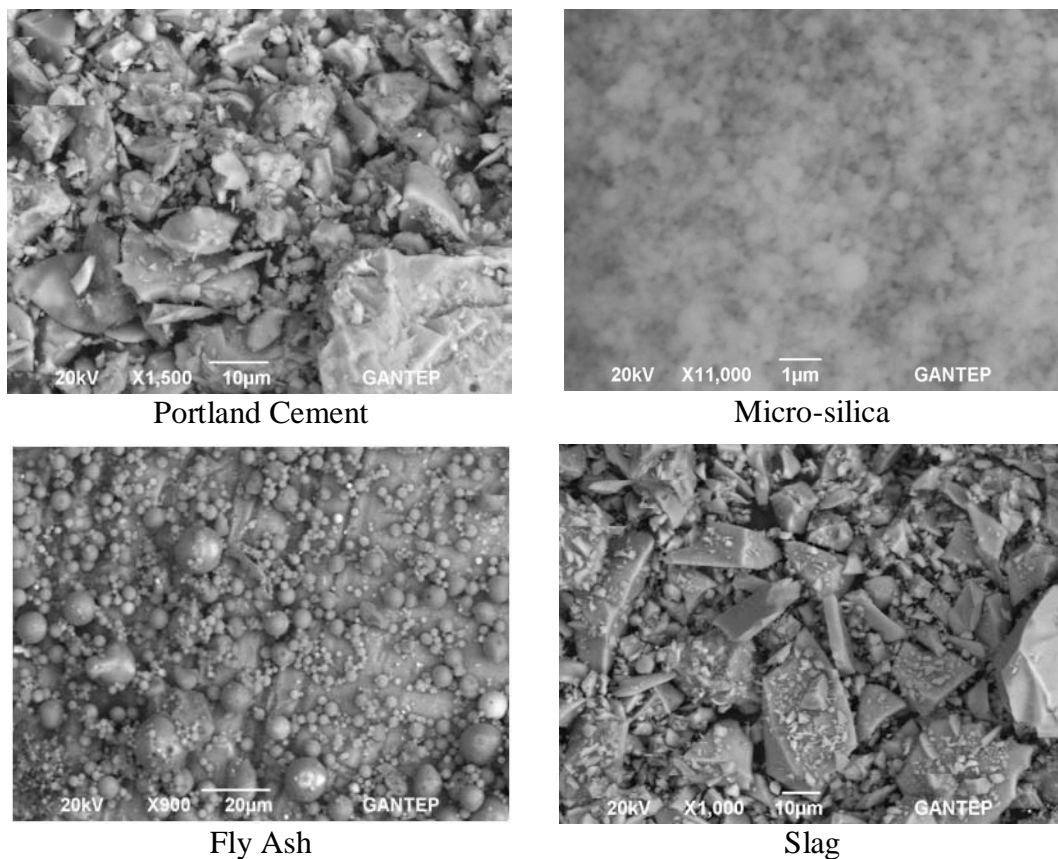


Figure 3.2 Particle morphology of Portland cement, micro-silica, fly ash and slag determined by SEM

3.1.3 Aggregate

In line with micromechanical design of ECC, it is necessary to have low matrix toughness for obtaining strain-hardening behavior and many closely spaced microcracks. However, with the increase of aggregate amount and size, toughness of the matrix increases and accordingly, maximum aggregate size that would be used in the mix is being restricted through this way (Li V.C., 1998). Therefore, in the production of ECC, to minimize the mortar matrix fracture toughness, no large aggregates were used and quartz sand with maximum aggregate size of 400 μm was incorporated to achieve certain characteristics successfully. Quartz sand with the maximum aggregate size (MAS) of 400 μm was obtained from local sources in our country's resources. Water absorption capacity and specific weight of quartz aggregate used is 0.3% and 2.60, respectively. The grain size distribution curves for these aggregates are presented in Figure 3.3.

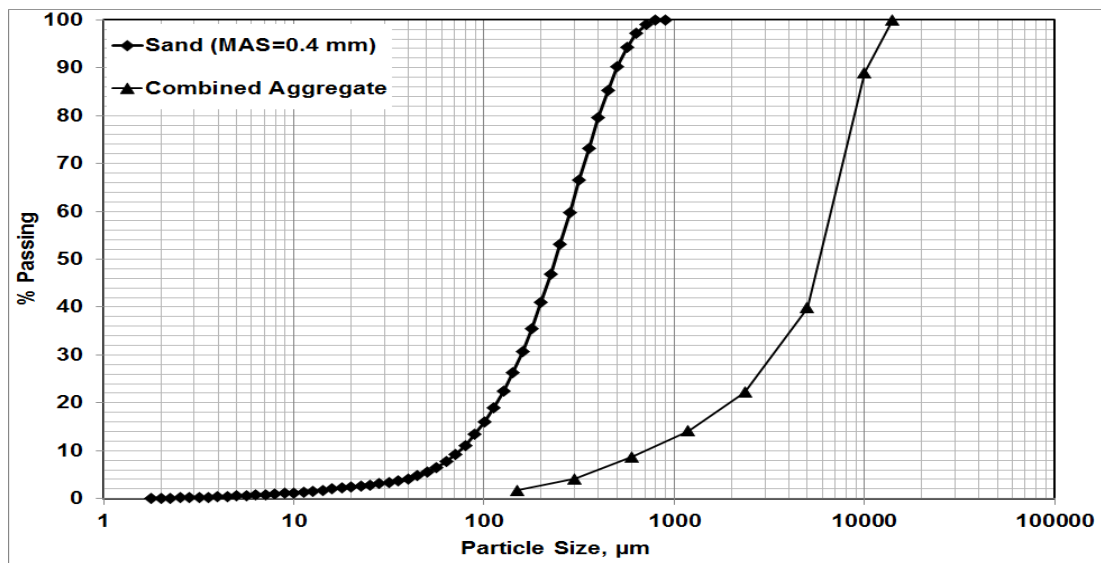


Figure 3.3 The grain size distribution curves for the aggregates used in this study

An aggregate combination of natural river sand with approximate particle size of 0.1 – 5 mm and crushed natural stone with 12 mm maximum size was used in the production of substrate concrete (SUBC) and micro-silica concrete (MSC) mixtures. Water absorption capacity and specific weight of this aggregate is 0.7% and 2.70, respectively. Particle size distribution of combined aggregates used in the production of SUBC and MSC is also given in Figure 3.3.

3.1.4 Chemical Admixtures

To improve the workability of ECC mixtures, Glenium 51, high range water reducing admixture (HRWR – polycarboxylate ether as an active ingredient with 1.1 specific gravity and 40% solid content) produced by BASF Construction Chemicals was used.

Two types of admixtures were used in the production of MSC and substrate concrete mixtures. Air entraining admixture (AEA) was used to protect them from freeze-thaw damage. Polycarboxylate ether based HRWR was added to reduce the amount of water required to obtain desired consistency of the mix.

3.1.5 Polyvinyl Alcohol (PVA) Fiber

Although various fiber types have been used in the production of ECC, PVA fiber was used in this study (Figure 3.4). The use of PVA fiber was decided based on and PVA-ECC represents the most practical ECC used in the field (Li et al., 2001; Kunieda and Rokugo, 2006) at the present.



Figure 3.4 PVA Fiber used in the production of ECC

PVA fibers have attracted most attention due to the outstanding composite performance and economics consideration. The dimensions of the PVA fiber are 8 mm in length and 39 μm in diameter. The nominal tensile strength of the fiber is 1620 MPa and the density of the fiber is 1300 kg/m^3 . The mechanical and geometric properties of PVA fibers are summarized in Table 3.2. The PVA fiber is surface-coated by hydrophobic oil (1.2% by weight) in order to reduce the fiber/matrix interfacial bond strength. To account for material inhomogeneity, a fiber content of 2% by volume in excess of the calculated critical fiber content has been typically used in the mix design. These decisions were made through ECC micromechanics material design theory and had been experimentally demonstrated to produce good ECC properties in previous investigations (Li et al., 2001; Kong et al., 2003a).

Table 3.2 Mechanic and Geometric Properties of PVA Fibers

Fiber Type	Nominal Strength (MPa)	Apparent Strength (MPa)	Diameter (μm)	Length (mm)	Young Modulus (GPa)	Strain (%)	Specific Weight kg/m^3
PVA	1620	1092	39	8	42.8	6.0	1300

3.2 Mixtures Proportions

In this study, a total of three overlay mixtures and one normal substrate concrete (SUBC) mixture were prepared. Mixture proportions are summarized in Table 3.3. The three overlay mixtures were: ECC with fly ash (F_ECC), ECC with ground granulated blast furnace slag (S_ECC) and microsilica concrete (MSC). The mixture proportion of an ECC mixture with FA (F_ECC) is the standard ECC mixture (M45) with properties extensively reported in the literature design (Wang and Li, 2007).

To increase the early age strength gain and ultimate strength, ECC mixture with slag (S_ECC), similar to F_ECC mixture except FA is replaced with slag, was also prepared. The MSC mixture was employed as control mixture. The choice and proportions of MSC mixture were based on the information collected from the literature. (Özyıldırım and Gomez, 1999; Sprinkel, 2000; Sprinkel, 2003; Sprinkel, 2004; Alhassan, 2007 and Mokarem et al., 2008) were studied about MSC as overlay

material. The mixture proportions and the mechanical and durability properties of concrete mixtures incorporating microsilica for overlay applications were comprehensively discussed in these studies. The test results show that MSC is one of the most effective and applicable with high performance material for rigid pavement overlay.

Table 3.3 Mixture proportions and main properties

Materials (kg/m³)	SUBC	MSC	F_ECC	S_ECC
Portland Cement	400	454	566	593
Micro-silica	-	45	-	-
Fly Ash	-	-	680	-
Slag	-	-	-	712
Water	180	150	331	347
Silica Sand	-	-	453	474
Coarse Aggregate	920	1068	-	-
Fine Aggregate	900	699	-	-
HRWR	1.8	5.5	5.0	6.0
AEA	0.43	0.43	-	-
PVA	-	-	26	26
Water/Binder	0.45	0.30	0.27	0.27
Slump flow (mm)	-	-	815	670
Air content (%)	5.3	4.7	6.9	6.4
Young's modulus (GPa)	25.8	35.2	19.7	24.9

The substrate concrete (SUBC) is a normal concrete usually used in the construction of rigid pavements, with a minimum compressive strength of 30 MPa and flexural strength of 4.5 MPa at 28 days (MDOT, 2009). It was prepared to determine the pavement overlay performances of F_ECC, S_ECC and MSC related to reflective cracking and flexural properties. The same mixture design was used for the concrete

in substrate portion of all specimens. The tested compressive and flexural strengths of substrate concrete at 28 days were 31 MPa and 5.0 MPa, respectively. The elastic modulus of each material was measured directly from compressive stress-strain curves for each material. Two strain gages were attached on a compression cylinder specimen 10 cm in diameter and 20 cm in height. The reported values in Table 3.3 are the average of three tests for each material.

Water to cementitious materials ratio (W/CM) in ECC mixtures was controlled at 0.27. Slight adjustments in the amount of HRWR admixture in ECC mixtures were made to achieve consistent rheological properties for better fiber distribution and workability. Both ECC mixtures had fresh properties similar to self-consolidating performance (Yang et al., 2009).

Table 3.3 shows that air content of air-entrained MSC is 4.7%, which is much lower than that for non-air entrained ECC mixtures. Although no air entraining admixture was added to ECC mixtures, air contents of these ECC mixtures in the fresh state as measured by ASTM C231 gave values in the range of 6-7%, which seemed to be adequate for freeze-thaw durability (ASTM C231, 1988). The apparently high air content in ECC mixtures may have resulted from the absence of coarse aggregate and the higher viscosity of the ECC in the fresh state (Şahmaran et al., 2009); the fine particles and high viscosity tend to prevent some of the air bubbles from rising to the surface during placing operations. The high workability used for all the mixtures would be good for pouring, and finishing of the overlays in the field. The specification of several departments of transportation is within this range of values for slump and air content.

In this study, a Hobart type mixer (Figure 3.5) with 20-liter capacity was used in preparing all ECC mixtures. Solid ingredients, including cement, mineral admixture (FA, S), and aggregate, were first mixed at 100 rpm for a minute. Water and HRWR admixture were then added into the dry mixture and mixed at 150 rpm for one minute and then at 300 rpm for another two minutes to produce a consistent and uniform ECC matrix (without PVA fiber). PVA fiber was added in last and mixed at 150 rpm for an additional three minutes.



Mixing of solid ingredients



Water addition



HRWR addition



Fiber addition

Figure 3.5 Production of ECC by using Hobart Type mixer

3.3 Specimens Preparation

All materials were tested in the freshly mixed state for slump flow and air content in accordance with relevant ASTM standards. Specimens were then prepared for tests in the hardened state. Several $\text{Ø}100 \times 200$ -mm cylinder specimens were prepared for compression testing and 400 (length) $\times 75$ (depth) $\times 80$ (height) mm prismatic specimens were prepared for four-point flexural strength testing. All specimens were demoulded at the age of 24 h, and moisture cured in plastic bags at $95 \pm 5\%$ RH, 23°C for 7 days as shown in (Figure 3.6). The overlay materials specimens were then air cured in laboratory at $50 \pm 5\%$ RH, 23°C until the age of testing.



Figure 3.6 Curing of ECC specimens after production of them

3.4 Test Procedure for Overlay Materials

3.4.1 Compressive Strength

Twenty four cylinder samples (6 specimens for each of age) of 100x200 mm were cast from each MSC, F_ECC and S_ECC mixtures. The compression test was carried out on the cylinder specimens by using a 3000 kN capacity testing machine in accordance with ASTM C39 (1988) (Figure 3.7). All of the samples were tested for compressive strength measurement at the age of 1, 7, 28 and 90 days. Before conducting this test, the top and bottom surfaces of the cylinder samples were become smooth by capping.



Figure 3.7 Compression testing machine with a cylinder sample

3.4.2 Flexural Performance

To measure the flexural performance of ECC and MSC mixtures, twenty four prismatic samples (6 specimens for each age of testing) having dimensions of 400x75x80 mm were cast from each produced ECC and MSC mixtures. Mixtures prisms were first cleaned, and then flexural strength under four-point test was performed by using universal testing system (Figure 3.8).



Figure 3.8 Four-point bending test

Four point bending test was performed on a closed-loop controlled material test system at a loading rate of 0.005 mm/s. The capacity of the loading frame was 100 kN (Figure 3.9). A four point bending loading fixture was developed to eliminate extraneous deformations such as support settlements and specimen rotations. The span length of flexural loading was 304 mm with a 101 mm center span length. During the flexural tests, the load and mid-span deflection were recorded on a computerized data recording system. Linear variable displacement transducer (LVDT) was fixed on the test set-up to measure the flexural deflection of the specimen. To evaluate composite performances, microstructural analysis in terms of scanning electron microscopy (SEM) and mercury intrusion porosimetry (MIP) were also performed on selected mixture. The results obtained from the mechanical tests

and microstructural analysis at the aggregate-matrix and fiber-matrix interfaces lead to a better understanding of behavior, and may be used in the improvement of mechanical performance and ductility of ECC.



Figure 3.9. Four-point flexural strength test

3.4.3 Drying Shrinkage

The drying shrinkage of bar specimens was measured up to 180 days after an initial curing of one day in the mould and 27 days in lime saturated water by using three 285×25×25 mm prismatic specimens in accordance with ASTM C157 (2004) for all ECC and MSC mixtures (Figure 3.10). Gauge studs were inserted in the bar moulds coaxial with the bar before the ECC and MSC mixtures were poured in to the moulds. The drying shrinkage specimens were stored in laboratory at 23 ± 2 °C, and $50\pm 5\%$ relative humidity.



Figure 3.10 Drying shrinkage device and samples

3.4.4 Restrained Ring Shrinkage

Although there is no standard test to assess cracking due to restrained shrinkage, several restrained shrinkage test methods have been proposed to measure the shrinkage cracking behavior of concrete (Malhotra, 1970; Kraai, 1985; Carlson and Reading, 1988). In this work, ring tests were used to assess the potential for restrained shrinkage cracking. Restraining ring was made of ECC and MSC mixtures (140 mm in height) cast around the outer perimeter of a steel ring with 280 mm and 305 mm inner and outer diameters, respectively. A 25.4 mm thick layer of ECC and MSC was cast around a 12.5 mm thick steel annulus. For each type of ECC and MSC mixtures, two rings were cast and cured in the molds for 24 hours. The exterior mold was removed 24 hour after casting and the top surface of the ring was sealed using a silicone-based sealant. The rings were then placed in an environmental chamber at $50 \pm 5\%$ relative humidity (RH) and 23 ± 2 °C. Therefore, drying was allowed only from the outer circumferential surface of the ring-type concrete for restrained shrinkage specimens. It should be noted that the curing conditions for the ring tests are different from the free drying shrinkage test. The purpose of the early demolding and short

curing time in the ring tests is to simulate the early re-opening conditions in field application. The restrained shrinkage was used to record the onset time of a new crack and the time development of the width at the crack mouth. The cracking pattern, crack number and crack width were measured as a function of age with a hand held microscope. Measurements were taken every 24 hour for 28 days at three different locations along each crack and the average value was plotted. A schematic restrained ring test setup is shown in Figure 3.11.

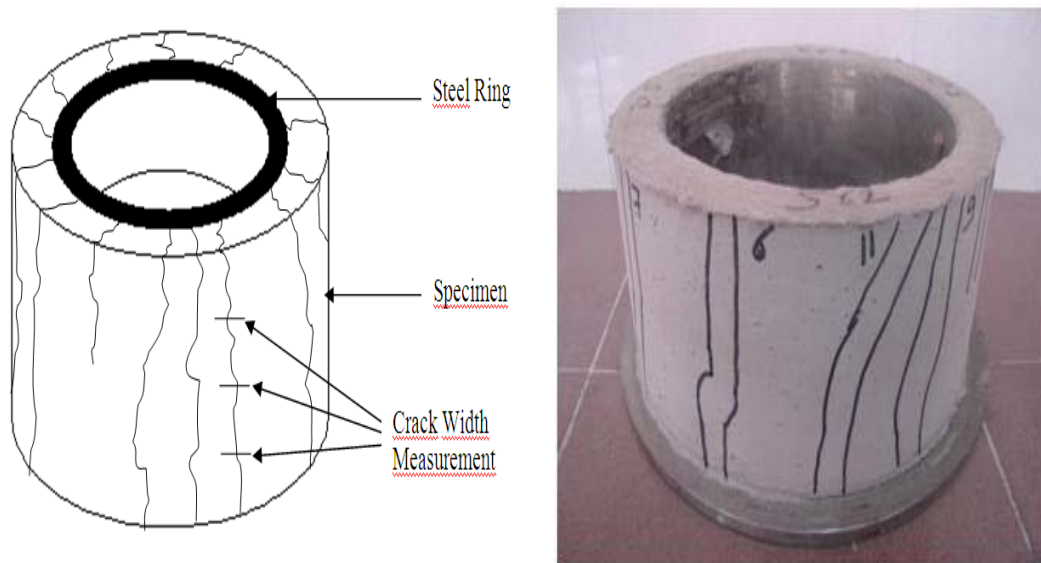


Figure 3.11 Restrained shrinkage test setup

3.5 Specimen Preparation and Testing for Flexural Performances and Reflective Cracking of Layered Specimens (Overlay+Substrate Concrete)

3.5.1 Flexural Performance of Layered Specimens

The first step in layered specimen preparation was to cast the 400x75x80 mm base member from substrate concrete (SUBC), which represents the old rigid pavement. After demoulding and 28-days basic curing in lime-saturated water, the substrates were left during 5 months in room with temperature of 23 °C and relative humidity of 50%. After that, specimens were cut with a diamond saw to catch the thickness of 30 mm (Figure 3.12).



Figure 3.12 Substrate specimen with 30 mm thickness after diamond saw cutting

This smooth diamond saw cut surface provides also the same surface condition of the substrate in each overlay system. Thus, 400x75x30 mm beam specimens were produced to use as concrete substrate. The overlay material was cast on the upper of the substrate material with three different thicknesses: 2.5 cm, 3.5 cm and 5.0 cm thickness (Figure 3.13).

A specimen consisted of a layer of overlay material on a substrate simulating the structure to be repaired. Three different overlay materials were used (MSC, F_ECC and S_ECC). To determine the flexural performance of layered overlay-substrate composite beams, four point bending tests were carried out with MSC, F_ECC and S_ECC overlay surface on the bottom (in tension) and SUBC surface on the top (in compression) as in the field condition. In each overlay type, eighteen specimens were cast over the concrete substrate with dimensions of 400x75x30 mm. All specimens were demolded after 24 hours, and moisture cured in plastic bags at 95 ± 5 % RH, 23 ± 2 °C for 7 days, and then, air cured at 50 ± 5 % RH, 23 ± 2 °C until the day of testing. Four point bending test was performed on a closed-loop controlled material testing system at a loading rate of 0.005 mm/s with the composite beams at the age of 1, 7 and 28 days. A four point bending loading fixture was developed to eliminate extraneous deformations such as support settlements and specimen rotations. The mid-point deflection was recorded with two linear variable differential transducers (LVDT) and it represents the relative displacement between the top of the beam and the loading fixture. The span length of flexural loading was 350 mm with a 116 mm center span length. During the flexural tests, both loading and mid-span deflection were recorded on a computerized data recording system.

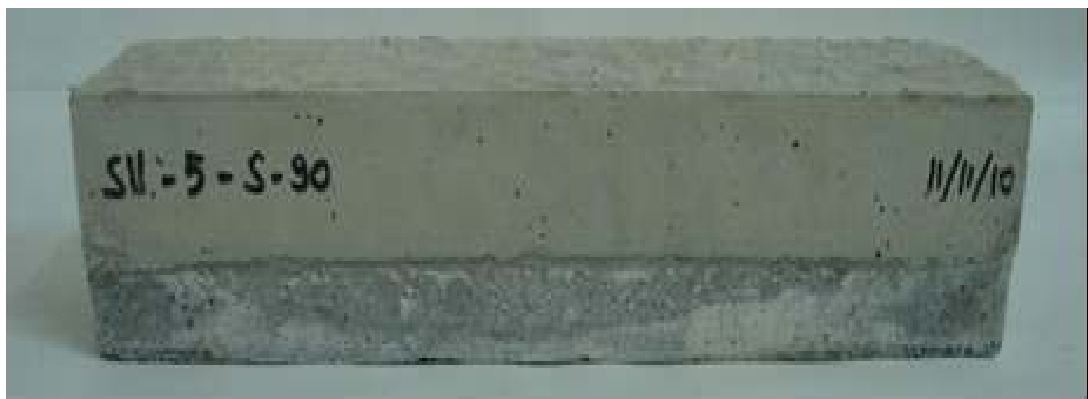
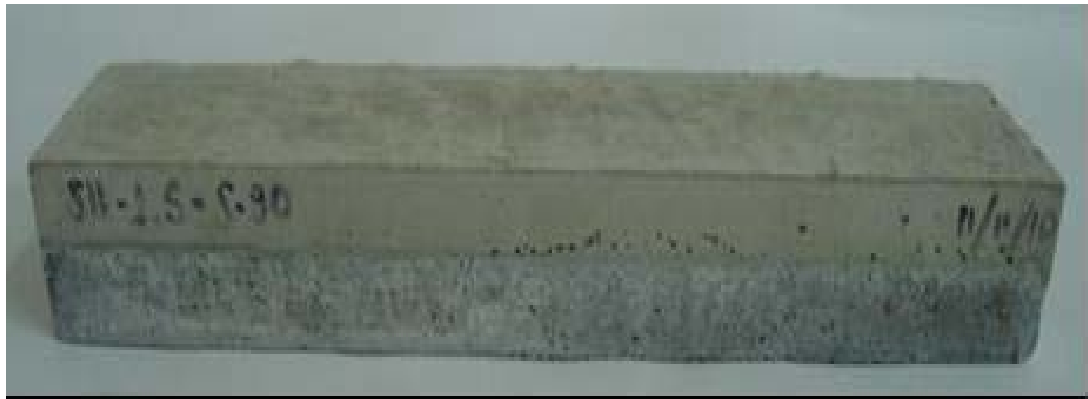


Figure 3.13 Layered specimens with different thicknesses for flexural performance

3.5.2 Reflective Cracking of Layered Specimens

Overlay is usually applied as a surface rehabilitation on deteriorated pavements, bridge decks, parking lots, airport pavements and industrial floors for riding quality or strengthening of existing pavement. These deteriorated infrastructures might contain cracks or joints, and these defects could be the initiation points of failures in rehabilitated systems. Reflective cracking in the overlay material above a joint in the original pavement is a commonly observed phenomenon of overlay failure. To simulate the reflective cracking in overlaid pavements, a composite beam, initially

used by (Lim and Li, 1997; Kamada and Li, 2000; Zhang and Li, 2002), is utilized with four-point bending load applied to the beam as a loading condition. The substrate concrete blocks were cut out of concrete beams with size 400x75x30 mm. These concrete beams were cut into the base blocks with a diamond saw. Each such beam was cut into two equal blocks with height 30 mm to form two substrate beams with preinduced joint (or substrate crack) at beam center. Only diamond saw cut surface against the overlay were used in this study.

The existing vertical cracks were made by using a smooth water-proof tape along the periphery of each substrate to form a notch prior to casting the overlay materials. After preparation of 30 mm thick smooth SUBC specimens with a vertical crack in the center of the beam (Figure 3.14), MSC, F_ECC and S_ECC mixtures were cast on these substrate concrete specimen with three different thicknesses, 25 mm, 35 mm and 50 mm.



Figure 3.14 Substrate specimen after cutting (30 mm thickness) with a vertical crack

All specimens were demoulded after 24 hours, and moisture cured under plastic bags at 95 ± 5 % RH, 23 ± 2 °C for 7 days. The specimens were then air cured at 50 ± 5 % RH, 23 ± 2 °C until the day of testing. Four-point bending test, which modeled in (Figure 3.15), was performed under displacement control at a loading rate of 0.005 mm/s with these composite specimens at the age of 7 and 28 days. Mid-point deflection was measured with two linear variable differential transducers (LVDT) that sat on the base part of the bending test fixture.

After the final failure of specimens, interface crack (extension) lengths were measured at both sides of a specimen as the distance from an initial notch tip to a propagated crack tip along the interface between the base concrete and the overlay material. Six specimens of each overlay material type and thickness were prepared for each testing age.

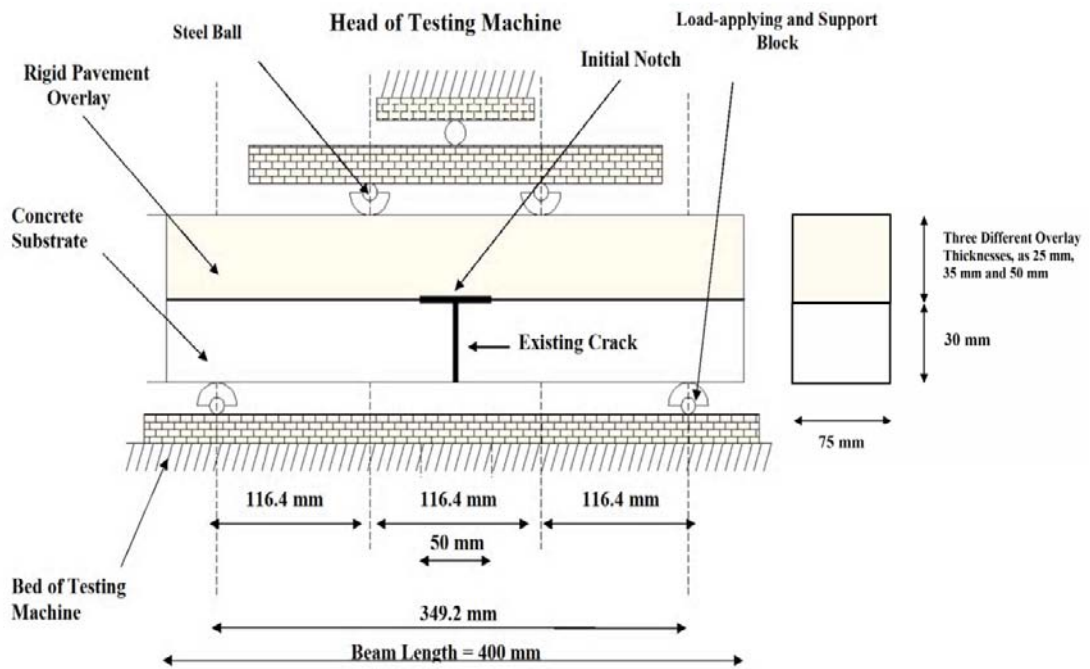


Figure 3.15 Model of four-point bending for reflective cracking test

CHAPTER IV

RESULTS AND DISCUSSIONS

4.1 Properties of Overlay Materials

4.1.1 Compressive Strength

Compressive strength is one of the mechanical properties of the substrate concrete and the overlay materials, which is shown in Table 4.1. At the ages of 1, 7, 28 and 90 days, compressive strength tests for cylinder specimens were applied following ASTM C39 procedures (1988). Table 4.1 tabulates the average of compressive strength results as determined from six cylinder specimens.

Table 4.1 Compressive Strength of overlay materials

Mix ID	Compressive Strength (MPa)			
	1 day	7 day	28 day	90 day
F_ECC	17.1	31.1	53.8	65.6
S_ECC	24.6	44.1	71.2	74.1
MSC	32.8	46.3	68.7	72.0
SUBC	-	-	31.9	-

As it is seen from Table 4.1, for the first 1 day of curing, strength gain in the MSC specimens was significantly higher compared to the ECC mixtures. At the ages of 7 days of curing, the compressive strength test results were similar for both S_ECC and MSC mixtures. However, the strength gain was more pronounced for S_ECC beyond 7 days of curing. Between the ages of 28 days and 90 days high amount of strength gain was achieved by F_ECC mixture, but still it has the lowest compressive strength at all ages. This finding was partially a result of the advances in hydration and pozzolanic reactions of the slag due to its large specific surface area (425 m²/kg surface area) compared to that of fly ash (290 m²/kg for FA).

Due to the smaller average particle size of slag than that of cement, it can well fill the space among the cement grains (filler effect), improving the particle distribution of cementitious system, and forming dense microstructure. Moreover, high surface area of slag provides more nucleating sites and OH^- ions as well as alkalis into the pore fluid (Roy and Idorn, 1983). This high strength should be correlated not only to the fineness but also to the self-cementitious activity of slag. The predominant reaction of slag with alkali hydroxide especially during the early hydration period seems to contribute to the strength of ECC mixture.

4.1.2 Flexural Strength

The direct tensile test is considered to be the most accurate method to confirm the strain-hardening behavior of a composite, as quasi-brittle fiber reinforced composites can potentially show apparent strain-hardening behavior under flexural loading, depending on the specimen geometry. However, previous studies demonstrate that deflection capacity under bending can be correlated with the tensile strain capacity when the material is truly strain hardening (Qian et al., 2009). Therefore, in this study, it was decided to use the four-point bending test to investigate the flexural strength and ductility of ECC mixtures.

Table 4.2 Flexural properties of overlay materials

Mix ID	Flexural Strength (MPa)				Deformation (mm)			
	1 day	7 day	28 day	90 day	1 day	7 day	28 day	90 day
F_ECC	5.35	8.80	11.51	11.82	4.18	4.78	4.43	3.99
S_ECC	6.74	10.89	12.04	12.58	3.18	3.23	3.05	2.94
MSC	4.97	6.30	7.00	7.56	0.55	0.41	0.28	0.27
SUBC	-	-	5.00	-	-	-	-	-

The test results in terms of flexural strength (MOR) and ultimate mid-span beam deflection at the peak stress at the end of 1, 7, 28 and 90 days are displayed in Table 4.2. Typical bending test results are displayed in Figure 4.1 in term of flexural stress–deflection diagrams for different kinds of overlay materials at the age of 28 days. The

flexural performances of overlay material mixtures were calculated by averaging the results of six specimens. As seen from Table 4.1, even though MSC mixture has the highest compressive strength at early ages, and similar compressive strength at later ages, the ECC prisms show a substantially higher ultimate flexural strength in comparison with that of the MSC prisms (Table 4.2). MOR of ECC mixtures values varied from 11.51 to 12.04 MPa showing that increase in the values of flexural strength of S_ECC was not that of drastic compared to the values of F_ECC for the first 28 days as in the compressive strength test results. Moreover, for all specimens, no significant flexural strength gain was observed beyond the age of 28 days. The most probable reason for this trend may be attributed to the fact that flexural strength is governed by more complex material properties, such as tensile first cracking strength, ultimate tensile strength and tensile strain capacity, particularly in the case of strain hardening cementitious materials (Şahmaran and Li, 2009b).

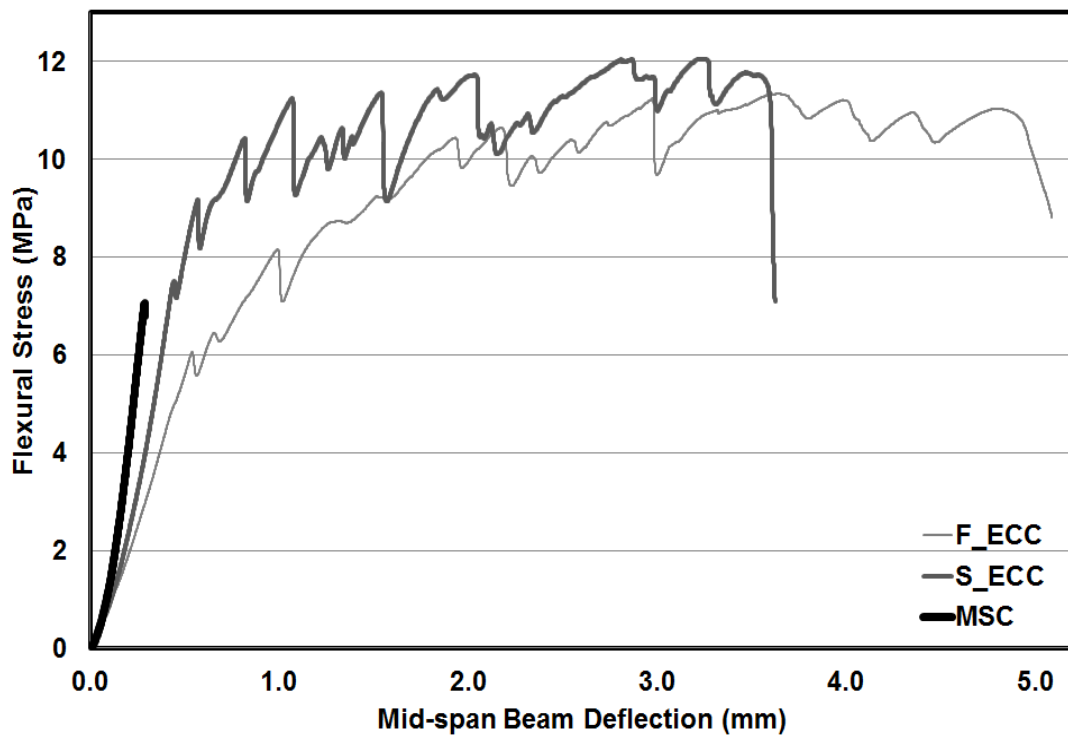


Figure 4.1 Flexural strength-mid-span beam deflection curves of overlay materials at 28 days of age

Ultimate mid-span beam deflection capacity, which reflects the material ductility, of the mixtures ranged between the values of 0.28 and 4.43 mm for the first 28 days. As seen from Figure 4.2, MSC mixture is a brittle material with sudden fracture failure, on the other hand, F_ECC and S_ECC samples have significantly higher deformation capability than MSC at all testing ages. Among the ECC mixtures, F_ECC showed the highest deflection capacity, therefore ductility, at all ages. The improvement in the mid-span beam deflection capacity with the use of Class-F FA can be attributed to the fact that the addition of FA has a tendency to reduce PVA fiber/matrix interface chemical bond and matrix toughness while increasing the interface frictional bond, in favor of attaining high tensile strain capacity (Wang and Li, 2007; Şahmaran and Li, 2009b). The overall decrease in the mid-span beam deflection capacity for S_ECC specimens might be associated with higher lime content and reactivity of slag which in turn causes enhanced fracture toughness, bond strength and the chemical bond between mortar matrix and fibers. Although S_ECC mixtures exhibit smaller deformation capacity, their flexural deflection capacity is still around or more than 3 mm at 28 days of age. The 3.0 mm deformation is nearly equivalent to almost 2.0% strain capacity on the tensile face of the beam. This deflection capacity remains almost 200 times higher than that in normal concrete and conventional fiber reinforced concrete (Qian and Li, 2008).

4.1.3 Drying Shrinkage

Free drying shrinkage tests were conducted on ECC and MSC (reference) prism specimens. The free drying shrinkage specimens were stored in a controlled environment at 23 ± 2 °C and $50 \pm 5\%$ relative humidity, and free shrinkage was recorded as the change in length over a gage length (distance between tips of gage studs) of 254 mm up to a test at the age of 180 days. The results of drying shrinkage test at the age of 180 days are shown in Figure 4.2. Each value in Figure 4.2 represents the average drying shrinkage measurements of three specimens. The ECC mixtures produced for this study had the same W/CM ratio, so varying water requirement was not a factor for drying shrinkage test results of ECC overlay materials.

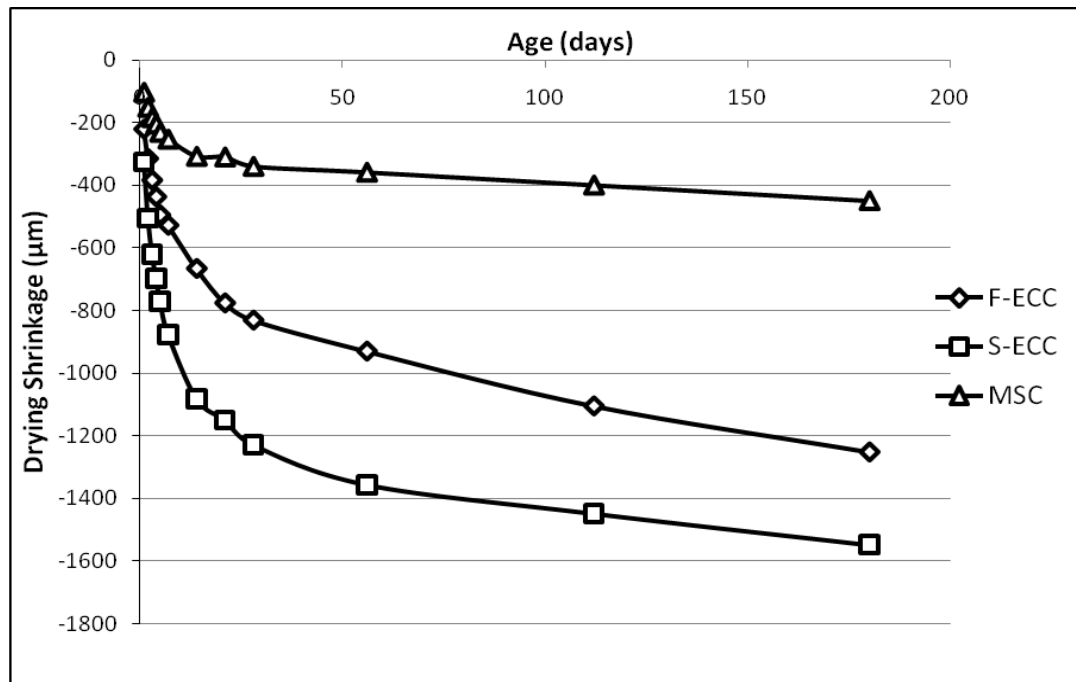


Figure 4.2 Drying shrinkages of overlay mixtures

The drying shrinkage strains at the age of 180 days ranged between 451 and 1548 micro-strain. ECC mixtures with slag exhibited the highest drying shrinkage of 1548 $\mu\epsilon$ at the end of 180 days. While by using FA with ECC can effectively reduce free drying shrinkage deformation. A possible mechanism contributing to the reduction of drying shrinkage in ECCs is the matrix densification due to FA addition, which may prevent internal moisture evaporation (Maslehuiddin et al., 1987). The matrix densification is typically attributed to the shape, pozzolanic property, and micro-filler effect of FA. An alternative mechanism is that unhydrated FA particles act as aggregates, which provide restraint to shrinkage, and the coarser pore structure, which results in decreased surface tension when a meniscus is formed and, thus, lower shrinkage forces exerted on the surrounding cement paste (Bisailon et al., 1994; Zhang, 1995; Şahmaran et al., 2007). On the other hand, compared with F_ECC mixtures, the use of partial volume replacement of Portland cement by slag can lead to increase ultimate drying shrinkage. For example, the shrinkage strain of mix S_ECC at the age of 180 days is 1548 $\mu\epsilon$, which is more than 19% higher than that of F_ECC. The increase in the drying shrinkage of ECC might be due mainly to pozzolanic reaction and enhanced pore size refinement mechanism of slag especially at earlier ages. Typical pore size distribution curves are shown in Figure 4.3 for the F_ECC and S_ECC mixtures.

As seen in Figure 4.3, the porosity of S_ECC was much lower and has finer sizes than F_ECC, which may proportionately increase free shrinkage.

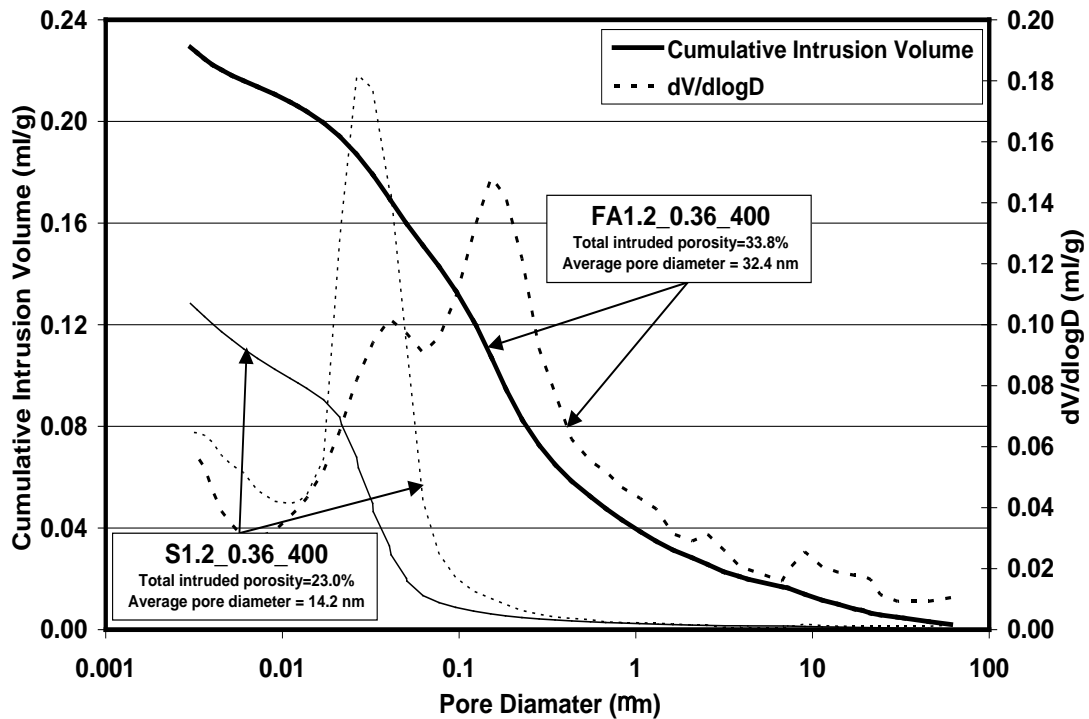


Figure 4.3 Comparison of pore size distribution of ECC mixtures with FA and slag at 28 days

The experimental results revealed also that the drying shrinkage of ECC overlay materials is above triple that of the MSC reference overlay mixture. This is due to the very high cementitious materials (Portland cement and mineral admixture) content, and absence of large volume of coarse aggregates. The previous results showed that the restraining effect of the micro-silica sand in the ECC mixtures was too small to contribute significantly to drying shrinkage (Şahmaran et al.,2009).

4.1.4 Restrained Shrinkage Cracking

Shrinkage cracking is a major problem for concrete structures, especially for flat structures, such as highway pavement, slabs and walls. Free shrinkage tests alone cannot offer sufficient information on the behavior of concrete structures because virtually every concrete structure is restrained in some way, either by reinforcement

or by the boundary condition of the structure. In this study, the method of the ECC and MSC rings cast next to a steel ring is used to simulate restrained shrinkage cracking. Once exposed to the ambient relative humidity and temperature conditions, the drying shrinkage deformation of the F_ECC, S_ECC and MSC, when restrained by the steel ring, results in internal radial pressure. Consequently, the overlay material layers are subjected to a circumferential tensile stress state that can cause cracking. The cracking pattern, crack number and crack width were measured as a function of age with a portable microscope. Measurements were taken at three different locations along each crack and the average value was plotted. From each overlay material, two specimens were tested. Crack numbers occurred on the F_ECC, S_ECC and MSC mixtures, and average, minimum and maximum crack widths are presented in Table 4.3.

Table 4.3 Restrained shrinkage crack characterization of overlay mixtures

Mixtures	Crack Width (μm)			Crack Number
	Average	Minimum	Maximum	
F_ECC	78	40	100	7
S_ECC	108	80	125	8
MSC	165	50	280	2

For the MSC control specimens, two cracks were observed in each specimen. The average and maximum crack width of the two specimens were 165 μm and 280 μm at 28 days. For F_ECC and S_ECC specimens, 7 and 8 cracks were formed at 28 days, respectively. The average crack widths at the end of 28 days were 78 μm and 108 μm for F_ECC and S_ECC specimens, respectively. The crack width of these ECC microcracks was significantly lower than the crack width of MSC localized cracks, and the former retains its load carrying capacity after crack formation. Restrained ring shrinkage tests results during 28 days period after casting are shown in Figure 4.4. Because of significant differences between these two crack widths, only maximum crack width of MSC specimens were considered in Figure 4.4. As seen in Figure 4.4, both ECC mixtures showed some degree of multiple cracking.

Basically, the width of a crack developed very fast in the first few days after crack formation. From then on the rate of development diminished its intension or stabilized. On the other hand, the crack width of MSC mixture still wants to go upward after 28 days.

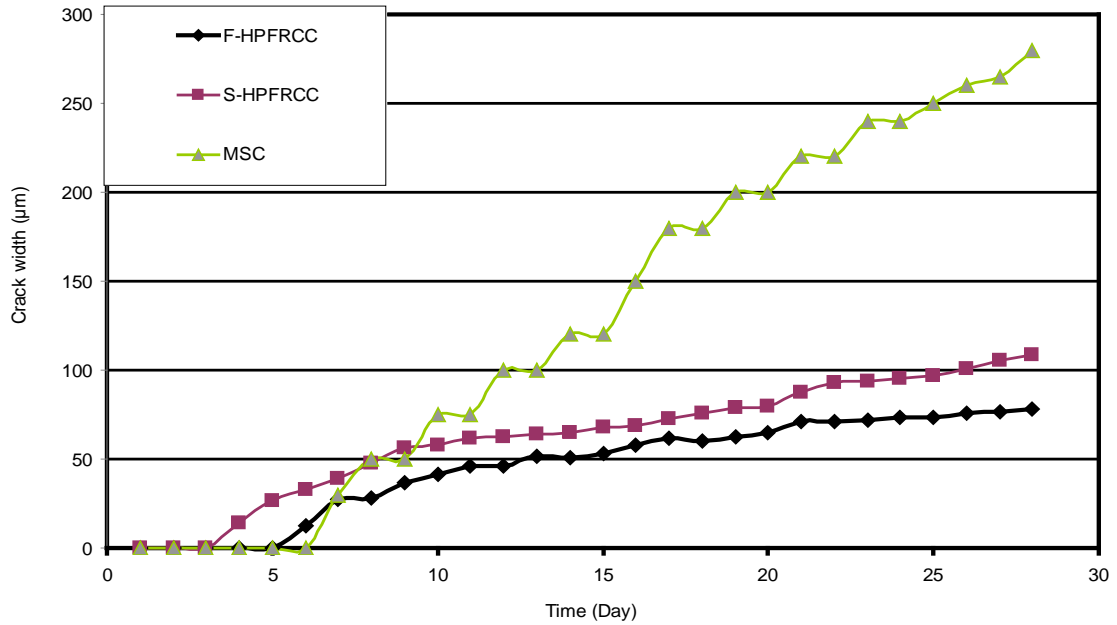


Figure 4.4 Crack width-time relations of overlay mixtures under restrained shrinkage

Wang et al. (1997) reported that as crack width increases from 100 µm to 500 µm, the permeability coefficient increases nearly seven orders of magnitudes from 1.0×10^{-11} m/sec to 1.0×10^{-4} m/sec. However, for crack widths under 100 µm, the permeability coefficient remains nearly identical to that of uncracked concrete, suggesting that for crack widths below this threshold there is no significant increase in permeability after cracking. Crack widths under 100 µm were also found to have same effective chloride diffusion coefficient as uncracked concrete (Sahmaran et al., 2007.). Taking these into account, the test results show that ECC overlay materials has significantly greater resistance to restrained shrinkage cracking than MSC, despite its higher drying shrinkage value. This is due to the large tensile strain capacity of ECC overlay materials, which leads to a negative shrinkage cracking potential and great dimensional compatibility with existing concrete.

4.2 Properties of Overlaid Specimens

4.2.1 Flexural Performance

The flexural test of layered specimens was conducted with three different overlay materials, namely F_ECC, S_ECC and MSC. Three overlay thicknesses of 25 mm, 35 mm and 50 mm were used for each material. Maximum flexural stress (or modulus of rupture) of F_ECC, S_ECC and MSC composite beams after four point bending test are summarized in Table 4.4.

Table 4.4 Flexural strengths of F_ECC, S_ECC and MSC composite beams after four point bending test

Mix ID	Thickness (mm)	Flexural Strength, MPa		
		1 day	7 days	28 days
F_ECC	25	4.83	7.55	9.46
S_ECC		6.30	8.94	10.88
MSC		4.64	5.33	6.07
F_ECC	35	5.12	8.12	9.98
S_ECC		6.31	9.90	11.00
MSC		4.80	5.59	6.22
F_ECC	50	5.29	8.50	11.31
S_ECC		6.58	10.48	11.98
MSC		4.85	6.11	6.51

The MSC test results serve as a reference for assessing the flexural performance of ECC overlaid specimens. The average flexural strength of substrate concrete beam was 5.0 MPa at the ages of 28 days. Test results showed that ECC overlaid specimens were superior to MSC overlaid specimens in terms of flexural strength regardless of the thickness of overlay. Among the ECC specimens, S_ECC composite beam has the highest flexural strength for each pavement overlay thickness and testing age. For 28 days of age the overlaying with 25 mm F_ECC, S_ECC or MSC on the diamond saw smooth interface offers respectively 9.46, 10.88 and 6.07 MPa in the flexural stress of layered specimen. The percentage of strength

improvement relative to the monolithic substrate concrete member is 89.2% for F_ECC, 117.6% for S_ECC and 21.4% for MSC overlay materials. The failure flexural stress is measured at 9.46 to 11.98 MPa treating the ECC overlay as an original monolithic ECC beam without the concrete substrate. Based on the results, it can be concluded that the addition of ECC layer could significantly improve the maximum flexural stress. Moreover, when the thickness of pavement overlay increases, the percentage of improvement with the use of ECC increased. It is important to note that, the maximum flexural load carrying capacities of 35 mm thickness ECC composite beams have a higher maximum flexural load carrying capacity than MSC composite beam with the thickness of 50 mm. In other words, in terms of load carrying capacity under flexural loading, ECC overlay materials with 35 mm thickness is preferable to MSC overlay with 50 mm thickness.

Figure 4.5 demonstrates the typical flexural stress mid-span beam deflection curves of the MSC, F_ECC and S_ECC pavement overlay composite beams with different overlay thicknesses as 25 mm, 35 mm and 50 mm at the ages of 28 days. As seen from Figure 4.5, in addition to the flexural strength improvement, the use of ECC layer can also result in significant ductility improvement for the layered beams. Strain-hardening behavior is appeared in every test case of F_ECC and S_ECC composite beams, but MSC composite beams show the behavior of brittle material. The F_ECC and S_ECC composite beams generally show increase in the amount of strain hardening, when the pavement overlay thickness increases. For 25 mm MSC composite beam, the average deflection capacity at ultimate stress was about 0.26 mm. With the addition of a 25 mm layer of S_ECC, this value increased to an average value of 2.2 mm, with a 746% increase as compared to that of micro-silica concrete. For the same overlay thickness, this value reached about 3.0 mm for F_ECC composite beam, which is about 1054% increase. If the thickness of pavement overlay increases to 35 mm, these values also increased as seen in Figure 4.5. The average deflection at ultimate load was about 0.27 mm, 3.0 mm and 3.5 mm for MSC, S_ECC and F_ECC, respectively. Therefore, the rise percentages of deflection at ultimate load were 1011% for S_ECC and 1196% for F_ECC. Also, for 50 mm pavement overlay thickness, the average deflection at ultimate load was about 0.29 mm for MSC, 3.5 mm for S_ECC with a 1106% increase and 4.1 mm for F_ECC with a 1313% increase.

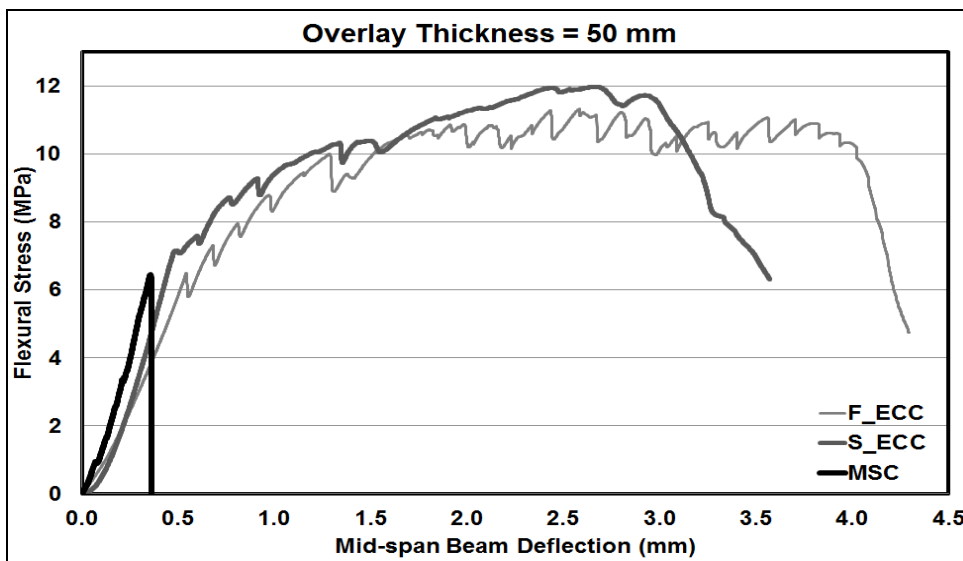
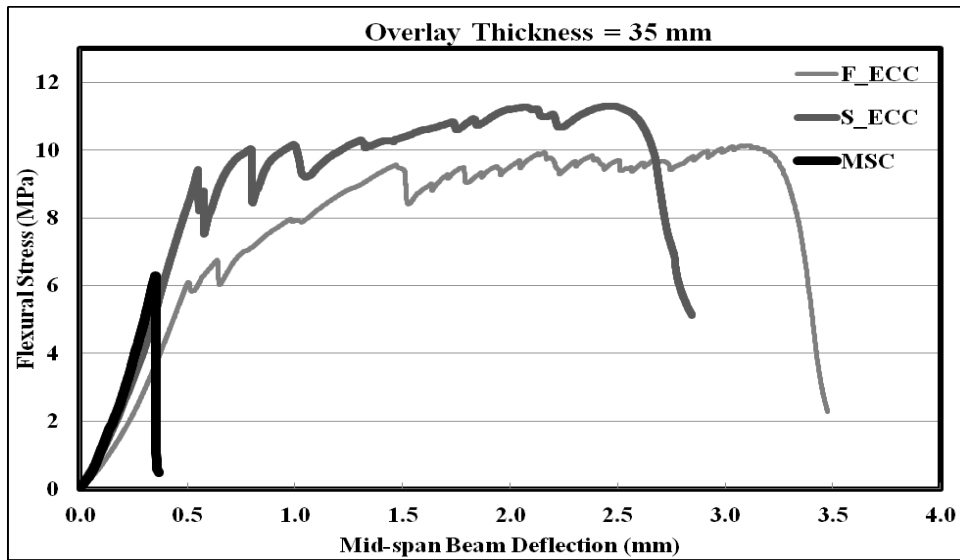
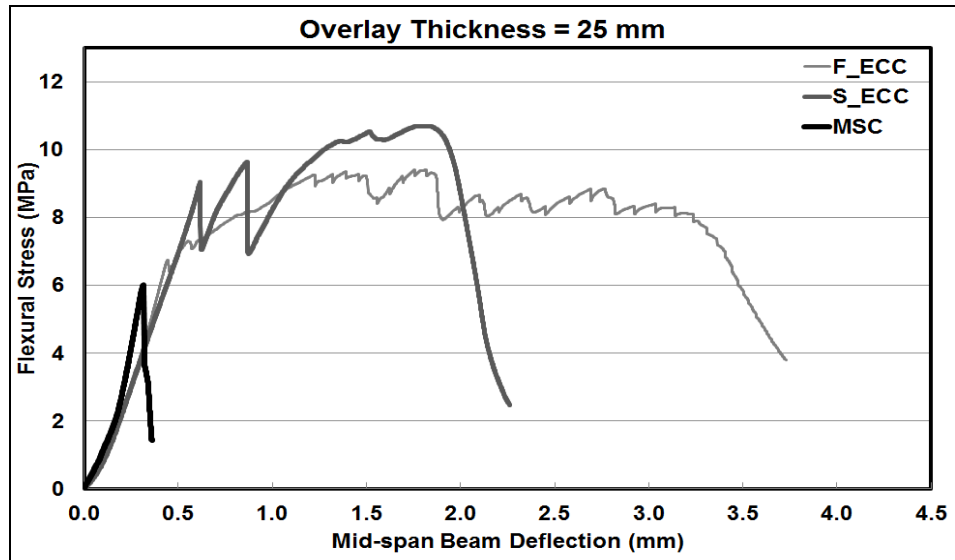


Figure 4.5 Load vs. deflection curves of pavement overlay mixtures with different thicknesses after four point bending test at the age of 28 days

The increase in deflection capacity with the use of ECC, which reflects materials' ductility, is related to change in the failure mode. The crack propagations of MSC, S_ECC and F_ECC composite beams after four point bending test can be seen in Figure 4.6. For MSC composite beam, there is only one major crack propagating from the bottom of the beam (Figure 4.6-a). For S_ECC and F_ECC composite beams, multiple fine cracks are formed in the ECC layer first (Figure 4.6-b and c). Finally, one of these cracks will open more widely than the others and propagate into the concrete layer. Multiple cracking permits large straining in the ECC layer until its failure, therefore leading to a higher ultimate deflection value and a ductile failure mode. Similar results were obtained from the previous work by using poly-ethylene fiber-reinforced ECC (Zhang and Li, 2002; Lim and Li, 1997; Kamada and Li, 2000). It is also important to note that both ECC overlay systems failed without delamination for all studied thicknesses in these experiments (Figure 4.6-a). However, regardless of the thickness of overlay, slight delamination between the substrate concrete and MSC overlay materials was observed (see Figures 4.6-b and c). Therefore, the deformation capacity of the material used in the overlay construction should be high enough to prevent the delamination type of failure in rehabilitated structures.



(a) MSC composite beam after four point bending test

Figure 4.6 Crack propagations of layered composite beams after four point bending test



(b) S_ECC composite beam after four point bending test



(c) F_ECC composite beam after four point bending test

Figure 4.6 (continued) Crack propagations of layered composite beams after four point bending test

4.2.2 Reflective Cracking Test

Table 4.5 summarizes the maximum flexural loads of F_ECC, S_ECC and MSC composite beams with three different pavement overlay thicknesses as 25 mm, 35 mm and 50 mm according to reflective cracking test. As seen from Table 4.5, as in

the flexural strength test results of overlaid specimens, S_ECC composite beam has the highest and MSC composite beam has the lowest maximum flexural load for each pavement overlay thickness and testing age.

Table 4.5 Maximum flexural loads of composite beams after reflective cracking test

Mix ID	Thickness (mm)	Maximum Flexural Load (N)	
		7 days	28 days
F_ECC	25	1066	1414
S_ECC		1409	1839
MSC		959	1278
F_ECC	35	2330	2857
S_ECC		3219	3652
MSC		1903	2108
F_ECC	50	4096	5486
S_ECC		5469	6780
MSC		3144	3334

In the ECC overlay system, in accordance with the type of ECC and overlay thickness, the ultimate load is approximately 1.1 to 2.0 times larger than that of the MSC overlay system. For 28 days of age and 25 mm overlay thickness, the maximum flexural load of MSC composite beam was 1278 N. For F_ECC composite beam this value increased to 1414 N, which is about 11% increase. For S_ECC composite beam, this value reached about 1839 N, which is about 44% increase. The tests results also show that there is a direct relationship between maximum flexural load and overlay thickness. When the thickness of pavement overlay increases as 35 mm and 50 mm, the percentages of increase are about 50% for F_ECC, 73% for S_ECC, and 82% for F_ECC, 103% for S_ECC, respectively. If pavement overlay thicknesses are compared, maximum flexural load of 35 mm thickness S_ECC composite beam has a higher maximum flexural load than MSC composite beam with the thickness of 50 mm. Therefore, as in the flexural performances, S_ECC mixture with the thickness of 35 mm can be used instead of 50 mm thick MSC mixture in accordance with the reflective cracking test results. The overall flexural

load-deflection behaviors as a result of reflective cracking testing in the three different overlay systems with different overlay thicknesses as 25 mm, 35 mm and 50 mm are illustrated in Figure 4.7. For the deflections at peak load, which reflect the system ductility and energy absorption capacity, the F_ECC and S_ECC composite beams are considerably larger than MSC composite beam. These results are in agreement with the previous results (Zhang and Li, 2002; Lim and Li, 1997; Kamada and Li, 2000). Besides, it is clear from Figure 4.7 that the energy absorption capacity in the F_ECC and S_ECC overlay systems are much enhanced when it is compared with MSC overlay system. The area under the load-deflection curve of the ECC overlay system is more than hundred times larger than that of the MSC overlay system. This meaningful improvement in ductility and energy absorption capacity of the F_ECC and S_ECC overlay systems are expected to improve the durability of repaired structures by resisting brittle failure. In many cases, the high ductility might be more important than the strength. The causes of failure in many infrastructures might be excessive uneven deflection in structures or imposed straining. The superior deflection capacity of the ECC overlay system can provide good serviceability without any major failure. According to the reflective cracking test results, when the pavement overlay thickness increases, the deflection values at ultimate load of F_ECC and S_ECC composite systems slightly decrease. This could be the effect of compression zone because in reflective cracking test, ECC overlay section of the composite beam face with compression zone unlike four point bending test of composite beams.

For all pavement overlay materials and thicknesses, F_ECC overlay system has the highest deflection capacity at ultimate load and MSC overlay system has the lowest deflection capacity at ultimate load, as seen in Figure 4.7. There is also a huge gap between the deflection values at ultimate load of ECC composite systems and MSC composite system. For instance, the deflection at ultimate load was about 0.3 mm for MSC composite beams, and the deflection at ultimate load was 4.9 mm and 3.6 mm for F_ECC and S_ECC composite beams, respectively for 25 mm pavement overlay thickness. This gap is related to change in the failure mode (see Figure 4.8).

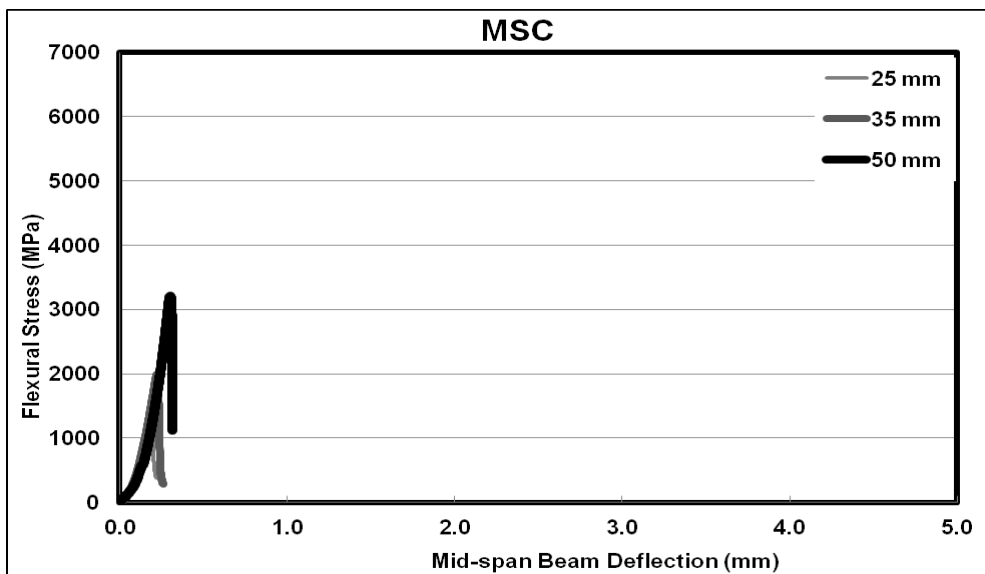
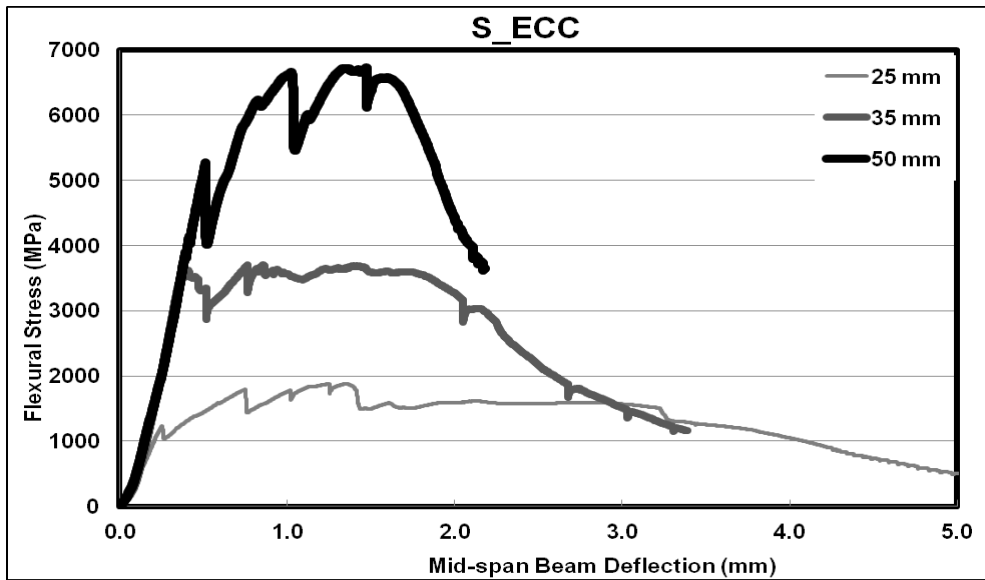
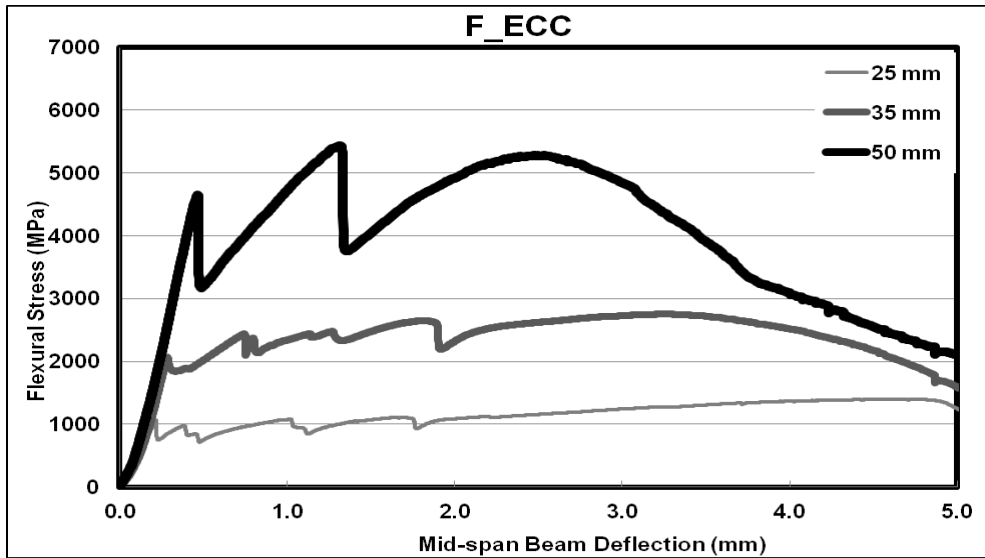


Figure 4.7 Load vs. deflection graph of pavement overlay mixtures after reflective cracking test at the age of 28 days

A typical crack patterns at failure of the composite beams with different overlay materials (F_ECC, S_ECC and MSC) are shown in Figure 4.8. The most significant differences in external appearance after testing between the ECC overlay systems and the MSC overlay system are the number of cracks and the crack width. In the MSC composite beams, only one crack at the initial notch in the overlay systems is found and this crack opening is the final failure of the MSC overlay system. The fractured halves of the specimens separated completely at the end of the test. However in the ECC overlay systems with smooth surface, for both ECC mixtures, multiple microcracks are developed on both sides of the initial notch increasing with the deflection of specimens (see Figure 4.8 a, and b). This means that the ECC overlay system was able to redistribute the load and utilize more material to resist the final failure. Multiple cracking also enables large deformation under flexural loading in the ECC layer before its failure, therefore leading to a higher ultimate deflection value and a ductile failure mode without direct crack reflection. It is also important to note that both the MSC and ECC overlay systems failed without delamination in these experiments (Fig. 4.6).



(a) S_ECC composite beam

Figure 4.8 Crack patterns at failure of overlay materials after reflective cracking test



(b) F_ECC composite beam



(c) MSC composite beam

Figure 4.8 (continued) Crack patterns at failure of overlay materials after reflective cracking test

The most significant differences in external appearance after testing between the F_ECC overlay system and the S_ECC overlay system are the crack number and the crack intervals. More multiple cracks are observed in the case of F_ECC with much

closer spacing. These observations are consistent with test results given in previous sections. Also the crack width in the ECC overlay systems (20 - 100 μm) is much smaller than the other overlay system (sub-millimeter for MSC) at the peak load. This is one of the outstanding characteristics of ECCs. Crack width control is of primary importance for many reinforced concrete applications, since it is believed that there is a close relationship between the mean or maximum crack widths and the durability of the structure. Moreover, the lower magnitude of the crack width is expected to promote the self-healing behavior, and thus the transport properties in cracked composites (Şahmaran et al., 2007; Şahmaran and Li, 2009a; Lepech and Li, 2005; Yang et al., 2005). Consequently, in the serviceability limit state a mean or maximum crack width less than about 0.1 mm is usually prescribed (Evardsen, 1999; Reinhardt and Jooss, 2003).

CHAPTER V

CONCLUSIONS

This thesis examines, on the basis of experimental results, the feasibility of using ultra-thin Engineered Cementitious Composites (ECC) overlay for the rehabilitation of rigid pavements. Two different ECC-overlay mixture designs are investigated: one with high strength and moderate ductility, and the other with moderate strength and high ductility. The rehabilitation work should desirably produce an overlaid pavement which has an improved resistance to reflective cracking, and a load-carrying capacity equal to or higher than the most effective and generally used as overlay material for rigid pavement overlay – microsilica concrete. The experiments were designed to study the properties of ECC overlays in two aspects: (i) dimensional stability of overlay materials in terms of drying shrinkage and restrained shrinkage, (ii) the flexural performances of ECC overlaid specimens with different thicknesses, and (iii) the reflective cracking characteristics of ECC overlaid specimens. The findings of the study are summarized below.

When the dimensional stability of individual overlay materials are compared, test results revealed that ECC mixtures with slag exhibited the highest drying shrinkage in comparison with the one that have fly ash. To compare ECC mixtures with MSC mixtures, the experimental results revealed that the drying shrinkage of ECC overlay materials is above triple that of the MSC reference overlay mixture. The test results also showed that ECC overlay materials has significantly greater resistance to restrained shrinkage cracking than MSC, despite it has higher drying shrinkage value.

Examining the performances of overlaid specimens under four-point flexural loading, significant differences between MSC overlay and ECC overlays with different thicknesses can be noted. First, it is clear that the flexural strength of the layered specimens is significantly increased by using the ECC material in the overlay

(above 100% of the value of MSC overlaid beam), and the degree of improvement increased with the thickness of ECC applied. Second, the deformation capacity, represented by midpoint deflection at peak load of the beams and energy absorption capacity, represented by the area under the load-deflection curve, with ECC overlaid are obviously increased in comparison to that of MSC overlaid beams. The difference between MSC and ECC overlaid beams on the deformability is due to the single cracking behavior of MSC in bending and the multiple cracking behavior of ECC in bending, respectively. The superior ductility of ECC is a desirable characteristic for it to replace MSC to suppress brittle failure. Third, the increase in deformability in the form of microcracking totally eliminates reflective cracking observed in substrate concrete overlaid with microsilica concrete. The ECC overlay system can also prevent the delamination type of failure in rehabilitated infrastructures. Finally, on the basis of the results of the test program presented, ECC overlay with 35 mm thick is superior to MSC overlay with 50 mm thick for rehabilitating concrete pavements. The superior performance of ultra-thin ECC overlay system under mechanical loading will be expected to prolong the service life of the structure under traffic loading and to reduce the costs in the rehabilitation work.

It is also important to note that the tests reported in this study do not provide a complete simulation of the actual loading, geometry and environmental conditions experienced by field situations. To increase confidence in predicting the behavior of ultra-thin ECC overlay system, however, the field-scale application of ECC as a repair material is needed to be carried out to obtain realistic and consistent results. The results reported in the present thesis provide a preliminary database of with ultra-thin ECC overlay behavior under flexural loading.

REFERENCES

- Alaee, F.J and Karihaloo, B.L. (2003) Retrofitting of RC beams with CARDIFRC. *ASCE Journal of Composites for Construction*, **7**, 174-186.
- Alhassan, M.A., (2007). Performance-based aspects and structural behavior of high performance fibrous bonded concrete overlays. *Thesis (Ph.D.)*. University of Illinois.
- American Society of Civil Engineers, (2009). *Report Card for America's Infrastructure - 2009*, American Society of Civil Engineers, Reston, Virginia, USA.
- ASTM C231, (1988). Test method for air content of freshly mixed concrete by the pressure method. *Annual Book of ASTM Standards*, **04.02**, 131.
- ASTM C39, (1988). Test method for compressive strength of cylindrical concrete specimens. *Annual Book of ASTM Standards*, **04.02**, 19.
- ASTM Standard C 666. (1991). Standard Test Method for Resistance of Concrete to Rapid Freezing and Thawing. *American Society for Testing and Materials*, Philadelphia, USA.
- ASTM Standard C 672. (2001). Standard Test Method Scaling Resistance of Concrete Surfaces Exposed to De-icing Chemicals. *American Society for Testing and Materials*, Philadelphia, USA.
- ASTM Standard C157. (2004). *Test method for length change of hardened hydraulic cement mortar and concrete*. American society for testing and materials. West Conshohocken, PA, USA.
- ASTM Standard C618. (2003). *Standard specification for coal fly ash and raw or calcined natural pozzolan for use in concrete*. American society for testing and materials. West Conshohocken, PA, USA.

ASTM Standard C989. (2009). *Standard specification for slag cement for use in concrete and mortars*. American society for testing and materials. West Conshohocken, PA, USA.

Battelle Group, (2002). *Towards a Sustainable Cement Industry*, World Business Council for Sustainable Development, Geneva, Switzerland.

Bisaillon, A., Rivest, M. and Malhotra, V.M. (1994). Performance of high-volume fly ash concrete in large experimental monoliths. *ACI Materials Journal*, **91**, 178-187.

Cable, J.K. and Hart, J., (1998). Evaluation of bond between ultra-thin PCC and asphaltic concrete. *Crossroads 2000 Proceedings*, Iowa State University, Ames Iowa, August.

Carlson, R.W. and Reading, T.J. (1988). Model study to shrinkage cracking in concrete building walls. *ACI Materials Journal*, **85**, 395–404.

Concrete Research and Education Foundation Strategic Development Council (CREFSDC), (2002) “Roadmap 2030: The US Concrete Industry Technology Roadmap” *Concrete Research and Education Foundation*, 2002, pp. 27.

Emmanuel, B.O.A., Lev, K. and Leslie, T. G., (1998). Mechanistic-based model for predicting reflective cracking in asphalt concrete-overlaid pavements. *Transportation Research Record*, 1629, 234–241.

Evardsen, C., (1999). Water permeability and autogenous healing of cracks in concrete. *ACI Materials Journal*, **96** (4), 448-454.

Fwa, T.F. and Paramasivam, P., (1990). Thin steel fibre cement mortar overlay for concrete pavement. *Cement and Concrete Composites*, **12**, 175-184.

Inaguma, H., Seki, M., Suka, K. and Rokugo, K. (2005). Experimental study on crack-bridging ability of ECC for repair under train loading. *Proc. Of Int’l Workshop on HPRCC in Structural Applications*, Honolulu, Hawaii, USA., pp. 499-508.

Kamada, T. and Li, V.C., (2000). The effects of surface preparation on the fracture behavior of ECC/concrete repair system. *Journal of Cement and Concrete Composites*, **22 (6)**, 423-431.

Kanda T. and Li, V.C., (1999). A new micromechanics design theory for pseudo strain-hardening cementitious composite. *ASCE Journal of Engineering Mechanics*, **124(4)**, 373-381.

Kendall, A., Lepech, M.D. and Keoleian G.A., (2008). Materials design for sustainability through life cycle modeling of Engineered Cementitious Composites. *Materials and Structures*, **41**, 1117-1131.

Kim, Y.Y., Kong, H.J. and Li, V.C. (2003). Design of Engineered Cementitious Composite (ECC) suitable for wet-mix shotcreting. *ACI Materials Journal*, **100**, 511-518.

Kong, H.J., Bike, S. and Li, V.C. (2003). Development of a Self-Consolidating Engineered Cementitious Composite - Employing Electrosteric Dispersion/Stabilization. *Journal of Cement and Concrete Composites*, **25**, 301-309.

Kraai, P.P. (1985). Proposed test to determine cracking potential due to drying shrinkage of concrete. *Concrete Construction*, **30**, 775-778.

Kunieda, M. and Rokugo, K., (2006). Recent progress of SHCC in Japan – required performance and applications. *Journal of Advanced Concrete Technology*, **4 (1)**, 19-33.

Lepech, M. and Li, V.C., (2007). Large Scale Processing of Engineered Cementitious Composites. *Accepted for publication in ACI Materials Journal*, July 2007.

Lepech, M.D. and Li, V.C., (2005). Water permeability of cracked cementitious composites. *Paper 4539 of Compendium of Papers CD ROM, ICF 11*, Turin, Italy, March.

- Li, V.C. (2003). On Engineered Cementitious Composites (ECC) - A Review of the Material and Its Applications. *Journal of Advanced Concrete Technology*, **1 (3)**, 215-230.
- Li, V.C. and Lepech, M.D., (2004). Crack Resistant Concrete Material for Transportation Construction, *Transportation Research Board 83rd Annual Meeting Compendium of Papers, Paper No. 04-4680*, Washington, DC, USA.
- Li, V.C. and Leung, C.K.Y. (1992). Theory of steady state and multiple cracking of random discontinuous fiber reinforced brittle matrix composites. *ASCE Journal of Engineering Mechanics*, **118**, 2246–2264.
- Li, V.C., (1993) From micromechanics to structural engineering – the design of cementitious composites for civil engineering applications. *JSCE Journal of Structure Mechanics and Earthquake Engineering*, **10 (2)**, 37-48.
- Li, V.C., (1997). ECC - Tailored composites through micromechanical modeling. *Fiber Reinforced Concrete*, 64-97.
- Li, V.C., (1998). ECC tailored composites through micromechanical modeling. *Fiber Reinforced Concrete: Present and the Future edited by Banthia et al*, CSCE, Montreal, pp. 64-97.
- Li, V.C., (2003b) "Durable Overlay Systems with Engineered Cementitious Composites (ECC)," *International Journal for Restoration of Buildings and Monuments*, **9(2)**, pp. 215-234.
- Li, V.C., Fischer, G., Kim, Y.Y., Lepech, M., Qian, S., Weimann, M. and Wang, S. (2003). Durable link slabs for jointless bridge decks based on strain-hardening cementitious composites. *Report for Michigan Department of Transportation RC-1438*.
- Li, V.C., Lepech, M., Wang, S., Weimann, M., and Keoleian, G., (2004). "Development of Green ECC Sustainable Infrastructure Systems", *to appear in Proceedings for International Workshop on Sustainable Development and Concrete Technology*.

- Li, V.C., Wang S. and Wu C., (2001). Tensile strain-hardening behavior of PVA-ECC. *ACI Materials Journal*, **98** (6), 483-492.
- Li, V.C., Wu, C., Wang, S., Ogawa, A. and Saito, T., (2002). Interface tailoring for strain-hardening polyvinyl alcohol-Engineered Cementitious Composite (PVA-ECC). *ACI Materials Journal*, **99**(5), 463-472.
- Lim, Y.M. and Li, V.C., (1997). Durable repair of aged infrastructures using trapping mechanism of engineered cementitious composites. *Journal of Cement and Concrete Composites*, **19**(4), 373-385.
- Lin, Z., Kanda, T. and Li, V.C. (1999). On interface property characterization and performance of fiber reinforced cementitious composites. *Concrete Science and Engineering, RILEM*, **1**, 173-184.
- Maalej, M., Hashida, T. and Li, V.C., (1995). “Effect of Fiber Volume Fraction on the Off Crack-Plane Fracture Energy in Strain-Hardening Engineered Cementitious Composites”, *Journal of the American Ceramic Society*, **78**(12), pp 3369-3375, 1995
- Malhotra, V.M. (1970). Concrete ring for the determination of tensile strength of concrete.” *ACI Materials Journal*,. **77**, 354–357.
- Malhotra, V.M., (1998). Role of supplementary cementing materials in reducing greenhouse gas emission. *CANMET Report MTL*, 98-03, 1998, 16 pp.
- Markovic, I., Walraven, J.C. and van Mier, J.G.M., (2004). Tensile behaviour of high performance hybrid fibre concrete. *Eds. Li et al., Fracture Mechanics of Concrete Structures*, 1113-1120.
- Marshall, D.B. and Cox, B.N. (1988). A J-integral method for calculating steady-state matrix cracking stresses in composites. *Mechanics of Materials*, **8**, 127–133.
- Maslehuddin, M., Saricimen, H. and Al-Mani, A. (1987). Effect of fly ash addition on the corrosion resisting characteristics of concrete. *ACI Materials Journal*, **84**, 42-50.

Mehta, P.K., (1998). Role of pozzolanic & cementitious by-products in sustainable development of the concrete industry. *6th CANMET/ACI/JCI Conference: Fly Ash, Silica Fume, Slag & Natural Pozzolans in Concrete*, 1998.

Michigan Department of Transportation, (2009). *MDOT Bridge Design manual*.

Mokarem. D.W., Lane. D.S., Özyıldırım. H.Ç. and Sprinkel. M.M., (2008). Measurement of early age shrinkage of Virginia concrete mixtures. *Final Report*. VTRC 08-R9.

Özyıldırım, Ç. and Gomez, J.P., (1999). High-performance concrete in a bridge in Richlands, Virginia. *Final Report*. VTRC 00-R6.

Proceedings of the JCI international workshop on ductile fiber reinforced cementitious composites (DFRCC), *Japan Concrete Institute*, October 2002.

Qian, S. and Li, V. C., (2008). Simplified inverse method for determining the tensile properties of strain hardening cementitious composites. *Advanced Concrete Technology*, **6 (2)**, 353–363.

Qian, S., (2007). Influence of Concrete Material Ductility on the Behavior of High Stress Concentration Zones, (*Ph.D.*) *Dissertation*. University of Michigan: Ann Arbor.

Qian, S., Zhou, J., Rooij, M.R., Schlangen, E., Ye, G. and Breugel, K.V., (2009). Self-healing behavior of strain hardening cementitious composites incorporating local waste materials. *Journal of Cement and Concrete Composites*. **31**, 613–621.

Ramm, W. and Bischoff M., (1998). Autogenous healing and reinforcement corrosion of water-penetrated separation cracks in reinforced concrete. *Nuclear Engineering and Design*. **179**, 191-200.

Reinhardt, H.W. and Jooss, M., (2003). Permeability and self-healing of cracked concrete as a function of temperature and crack width. *Cement and Concrete Research*, **33 (7)**, 981-985.

Research and Innovative Technology Administration (RITA), (2008). *Transportation Statistics Annual Report*, US Department of Transportation, Washington, DC, USA.

Risser, R.J., LaHue, S.P., Vogit, G.F. and Mack, J.W., (1993). Ultra-thin concrete overlays on existing asphalt pavement. *Proceedings of the Fifth International Conference on Concrete Pavement Design and Rehabilitation*, 2, Purdue University, West Lafayette, Indiana, 247-254.

Rossi, P. and Parant, E., (2005). Mechanical behaviours of a multi-scale fibre reinforced cement composite (MSFRCC) subjected to severe loading conditions. *Eds. Banthia et al., Proceedings of Construction Materials*.

Roy, D.M. and Idorn, G.M., (1983). Hydration, structure, and properties of blast furnace slag cements, mortars, and concrete. *ACI Journal*, **79** (6), 445-457.

Şahmaran, M. and Li, V.C. (2007). De-icing salt scaling resistance of mechanically loaded Engineered Cementitious Composites. *Cement and Concrete Research*, **37**, 1035-1046.

Şahmaran, M. and Li, V.C., (2009a) "Influence of microcracking on water absorption and sorptivity of ECC," *Materials and Structures*, **42**, 593-603, 2009.

Şahmaran, M. and Li, V.C., (2009b). Durability properties of micro-cracked ECC containing high volumes fly ash. *Journal of Cement and Concrete Research*, **39**, 1033-1043.

Şahmaran, M., Lachemi, M., and Li, V.C., (2009). Assessing the durability of Engineered Cementitious Composites under freezing and thawing cycles. *Journal of ASTM International*, **6**, 1–6.

Şahmaran, M., Lachemi, M., Hossain, K. M. A., Ranade, R. and Li, V. C. (2009). Influence of Aggregate Type and Size on the Ductility and Mechanical Properties of Engineered Cementitious Composites. *ACI Materials Journal*, **106** (3), 308-316.

Sahmaran, M., Li, M., and Li, V. C., (2007) "Transport Properties of Engineered Cementitious Composites Under Chloride Exposure," *ACI Materials Journal*, Vol.**104**, No. **6**, pp. 604-611.

- Şahmaran, M., Yaman, İ. Ö. and Tokyay, M. (2007). Development of High Volume Low-Lime and High-Lime Fly-Ash-Incorporated Self Consolidating Concrete. *Magazine of Concrete Research*, **59**, 97-106.
- Sikdar, P.K., Jain, S.S., Bose, S., and Kumar, P., (1999). Premature cracking of flexible pavements. *Journal of Indian Roads Congress, Paper No. 461*, **60 (3)**, 355-398.
- Sprinkel, M., (2000). Evaluation of latex-modified and silica fume concrete overlays placed on six bridges in Virginia. *Final Report*. VTRC 01-R3.
- Sprinkel, M., (2003). Evaluation of corrosion inhibitors for concrete bridge deck patches and overlays. *Final Report*. VTRC 03-R14.
- Sprinkel, M., (2004). Performance specification for high performance concrete overlays on bridges. *Final Report*. VTRC 05-R2.
- Stang, H. and Li, V.C. (1999). *Extrusion of ECC-material*. In Proc. Of High Performance Fiber Reinforced Cement Composites 3 (HPFRCC 3) edited by H. Reinhardt and A. Naaman, Chapman & Hull, pp. 203-212.
- Suthiwarapirak, P., Matsumoto, T. and Kanda, T. (2002). Flexural fatigue failure characteristics of an Engineered Cementitious Composite and Polymer Cement Mortars. *Materials, Concrete Structure Pavements*, **57**, 121-134.
- Wang, K., Jansen, D, Shah, S. and Karr, A., (1997) "Permeability Study of Cracked Concrete," *Cement and Concrete Research*, Vol. **27**, No. **3**, pp. 381-393.
- Wang, S. and Li, V.C. (2004). Tailoring of pre-existing flaws in ECC matrix for saturated strain hardening. *Proceedings of FRAMCOS-5*, Vail, Colorado, USA, pp. 1005–1012.
- Wang, S. and Li, V.C., (2007). Engineered Cementitious Composites with high-volume fly ash. *ACI Materials Journal*, **104 (3)**, 233-241.
- Weimann, M.B. and Li, V.C. (2003b). Hygral behavior of engineered cementitious composites (ECC). *International Journal for Restoration of Buildings and Monuments*, **9**, 513-534.

Weimann, M.B. and Li, V.C., (2003a). Drying Shrinkage and Crack Width of ECC, *Seventh International Conference on Brittle Matrix Composites*, pp. 37-46, Warsaw, Poland.

Yang, E., Şahmaran, M., Yang, Y. and Li, V.C., (2009). Rheological control in the production of Engineered Cementitious Composites. *ACI Materials Journal*, **106 (4)**, 357–366.

Yang, Y., Lepech, M.D. and Li, V.C., (2005). Self-healing of ECC under cyclic wetting and drying. *Proceedings of Int'l Workshop on Durability of Reinforced Concrete under Combined Mechanical and Climatic Loads*, Qingdao, China, 231-242.

Yang, Y., Lepech, M.D., Yang, E. and Li, V.C., (2009). Autogenous healing of Engineered Cementitious Composites under wet–dry cycles. *Cement and Concrete Research*, **39(5)**, 382-390.

Zhang, H., Keoleian, G.A. and Lepech, M.D., (2008). An integrated life cycle assessment and life cycle analysis model for pavement overlay systems. *First International Symposium on Life-Cycle Civil Engineering*, Varenna, Lake Como, Italy: CRC Press/Balkema.

Zhang, J. and Li, V.C., (2002). Monotonic and fatigue performance in bending of fiber reinforced engineered cementitious composite in overlay system. *Journal of Cement and Concrete Research*, **32 (3)**, 415-423.

Zhang, M.N. (1995). Microstructure, crack propagation, and mechanical properties of cement pastes containing high volumes of fly ashes. *Cement and Concrete Research*, **25**, 1165-1178.